MICROCOPY RESOLUTION TEST CHART

REPORT DOCUMENTATION PAGE

DTIC FILE COPY

1a. REPORT SECURITY CLASSIFICATION UNCLASSIFIED			1b. RESTRICTIVE MARKINGS			
2a. ...FICATION AUTHORITY			3. DISTRIBUTION/AVAILABILITY OF REPORT Approved for public release; distribution unlimited.			
2b. ...N/DOWNGRADING SCHEDULE						
4. ...ANIZATION REPORT NUMBER(S)			5. MONITORING ORGANIZATION REPORT NUMBER(S) AFOSR-TR- 87-1669			
6a. ...IMING ORGANIZATION		6b. OFFICE SYMBOL *(If applicable)*	7a. NAME OF MONITORING ORGANIZATION Air Force Office of Scientific Research/NL			
6c. ...te, and ZIP Code)			7b. ADDRESS *(City, State, and ZIP Code)* Building 410 Bolling AFB, DC 20332-6448			
8a. ...G/SPONSORING		8b. OFFICE SYMBOL *(If applicable)* NL	9. PROCUREMENT INSTRUMENT IDENTIFICATION NUMBER AFOSR-86-0182			
8c. ADDRESS *(City, State, and ZIP Code)* Building 410 Bolling AFB, DC 20332-6448			10. SOURCE OF FUNDING NUMBERS			
			PROGRAM ELEMENT NO. 61102F	PROJECT NO.	TASK NO.	WORK UNIT ACCESSION NO.

AD-A188 395

11. TITLE *(Include Security Classification)*

12. PERSONAL AUTHOR(S)

13a. TYPE OF REPORT Reprint	13b. TIME COVERED FROM ___ TO ___	14. DATE OF REPORT *(Year, Month, Day)*	15. PAGE COUNT

16. SUPPLEMENTARY NOTATION

17.	COSATI CODES		18. SUBJECT TERMS *(Continue on reverse if necessary and identify by block number)*
FIELD	GROUP	SUB-GROUP	

19. ABSTRACT *(Continue on reverse if necessary and identify by block number)*

DTIC
ELECTED
NOV 2 4 1987
S
D

20. DISTRIBUTION/AVAILABILITY OF ABSTRACT ☒ UNCLASSIFIED/UNLIMITED ☒ SAME AS RPT ☐ DTIC USERS	21. ABSTRACT SECURITY CLASSIFICATION UNCLASSIFIED	
22a. NAME OF RESPONSIBLE INDIVIDUAL Dr. William Berry	22b. TELEPHONE *(Include Area Code)* (202) 767-5021	22c. OFFICE SYMBOL NL

DD FORM 1473, 84 MAR   83 APR edition may be used until exhausted.   SECURITY CLASSIFICATION OF THIS PAGE
All other editions are obsolete.   UNCLASSIFIED

87 11 14 100

Computer and Information Science

Simulation of a Classically Conditioned Response:
Components of the Input Trace
and a Cerebellar Neural Network Implementation
of the Sutton-Barto-Desmond Model

Diana E. J. Blazis and John W. Moore

COINS Technical Report 87-74
September 14, 1987

University of Massachusetts
Amherst, Massachusetts 01003

2 9 SEP 1987

Summary

The Sutton-Barto-Desmond (SBD) implementation of the Sutton-Barto model of connectionist learning describes many features of rabbit nictitating membrane response (NMR) conditioning. The rabbit NMR has been widely adopted as a model system for theoretical and neurobiological investigations of mammalian learning. The present report explores parameter sensitivity of the SBD model in the context of forward-delay conditioning with a single conditioned stimulus (CS). Constraints on the model's parameters are potentially useful in elucidating neural ssubstrates of NMR conditioning: Neural implementations suggested by the SBD model provide a framework for investigations of connectionist learning mechanisms at both the circuit and cellular level.

A fundamental assumption of the SBD model is that the input of a CS to the learning element is *shaped* by as-yet-unspecified coding processes such that the element's output conforms to the topography of response waveforms observed in the laboratory. Simulation experiments were conducted with various combinations of parameters that shape the CS representation. In addition to response topography, the model's performance was assessed in terms of rate and terminal levels of learning, simulated interstimulus interval functions, and other criteria. Implications of these experiments for possible brain mechanisms involved in processing and representing CS information are discussed.

Simulation results indicate that the SBD model's ability to capture major features of NMR conditioning is highly constrained by parameters that shape the CS. Taken together with experimental evidence implicating the cerebellum in NMR conditioning, these and other constraints on the model's parameters suggest various neural circuits for implementing the SBD learning rule. A class of circuit models favored by several theorists assume that learning occurs at synapses where parallel fibers convey CS information to cerebellar Purkinje cells. An alternative approach, elaborated in this report, assumes that learning occurs at synapses where mossy fibers convey CS information to cerebellar granule cells. This hypothesis was suggested by the invariance of a key parameter of the model: The time constant of the process governed by this parameter matches that of Golgi cell inhibition of granule cells. A circuit model based on this assumption can account for patterns of CR-related activity observed in single-unit recording studies.

Contents

Introduction

Workers in the behavioral and neurosciences have developed a fruitful approach to modeling brain function by combining mathematics with neurophysiology and anatomy (Churchland, 1986). This approach, sometimes referred to as computational neuroscience, provides a framework for integrating seemingly divergent areas of scientific inquiry. A particular example is the extension of a general mathematical model of learning to a specific instance of behavioral learning such as classical conditioning. Although most models represent the cumulative effects of conditioning without reference to motor output, we have shown how a *template* of the classically conditioned nictitating membrane response (NMR) of the rabbit can be incorporated into the neurally inspired model of classical conditioning proposed by Sutton and Barto (Barto and Sutton, 1982; Sutton and Barto, 1981). The original Sutton-Barto (SB) model was presented in the context of the extensive behavioral literature on NMR conditioning (see Gormezano, Kehoe, and Marshall, 1983). In essence, the approach we used resulted in an implementation of the SB model that not only describes cumulative effects of training but also response topography (Blazis, Desmond, Moore, and Berthier, 1986; Moore, Desmond, Berthier, Blazis, Sutton, and Barto, 1986). Models of NMR topography based on other theoretical frameworks have also recently been described (Desmond, Blazis, Moore, and Berthier, 1986; Desmond and Moore, 1987; Schmajuk, 1986; Schmajuk and Moore, 1986).

The rabbit NMR is a protective response resulting from retraction of the eyeball and the passive sweeping of the NM over the eye (Berthier, 1984; Berthier and Moore, 1980). The conditioned NMR is a graded, adaptive response. It has been employed for theoretical, behavioral, physiological, and anatomical investigations of learning in several laboratories. Our strategy for modeling the NMR was to constrain the SB model to predict response topography in a simple conditioning situation. Constraints were derived partly from electrophysiological experiments conducted in awake, behaving rabbits (Desmond, 1985). We have shown that the physiologically constrained SB model retains the ability of the original implementation to describe multiple-CS phenomena such as blocking, conditioned inhibition, and higher-order conditioning. These more complex learning situations are predicted without further modification of the parameters of the model (Blazis et al, 1986; Moore et al, 1986). We refer to this variant of the SB model as the Sutton-Barto-Desmond (SBD) model.

The present report describes simulation experiments with the SBD model that explore its sensitivity to parameters that control CS representation in single-CS forward-delay conditioning paradigms (Moore and Gormezano, 1977). We describe approaches to neural network implementations that integrate information about parameter sensitivity with

anatomical evidence indicating that cerebellum is essential for the conditioned NMR.

The Model

The SB adaptive element can be viewed as a neuron-like device capable of receiving input from many potential CSs. In Figure 1 these are designated as CS_i, i=1, ..., n. Each CS_i gives rise to a representation that provides a synaptic input, designated x_i to the element, and has a variable synaptic weight or efficacy, designated V_i. The unconditioned stimulus (US) is signaled by a pathway of fixed efficacy, designated λ. The output of the element, s, is the weighted sum of its inputs. Tesauro (1986) has criticized the SB model on the grounds that it is only applicable in situations where inputs are represented locally. However, Sutton and Barto (1987) point out that the SB model is also applicable when inputs are given a distributed representation.

Learning in the SBD model occurs according to a modified Hebbian rule (Sutton and Barto, 1981). Hebbian rules typically assume that learning can be reduced to modification of synaptic weights. They generally state that learning is a function of the *product* of synaptic activity evoked by a CS and the neuron's activity or output. In forming a mental picture of how a neuron "becomes conditioned" one usually imagines that it is relatively inactive unless fired by the US. If this US-evoked firing coincides with excitation from the CS input, the efficacy of this input pathway increases. This conceptualization of Hebbian learning obscures an essential point, namely, that changes of the CS's synaptic weight might occur at any moment before, during, and after the occurrence of the US, depending only on the element's activity during application of the CS. This activity might be spontaneous or evoked by other synaptic inputs including those from other CSs. Real-time Hebbian rules such as the SBD model are sensitive to this point because they allow for continual changes of synaptic weight.

Input

Our approach to extending the SB model to CR topography is to treat the input of the ith CS to the element, x_i, as a continuous function of time. The original SB model specified x_i as a rectangular pulse defined by the onset and offset of the CS. With no further processing, such an input produces a square wave output and with 0 latency. In contrast, a real conditioned NMR begins well after CS onset and rises gradually in a ramped or S-shaped fashion within the CS-US or interstimulus interval (ISI). The CR attains a maximum at or near the temporal locus of the US, and then decays rapidly during the post-US period. This pattern of response topography is also reflected in the
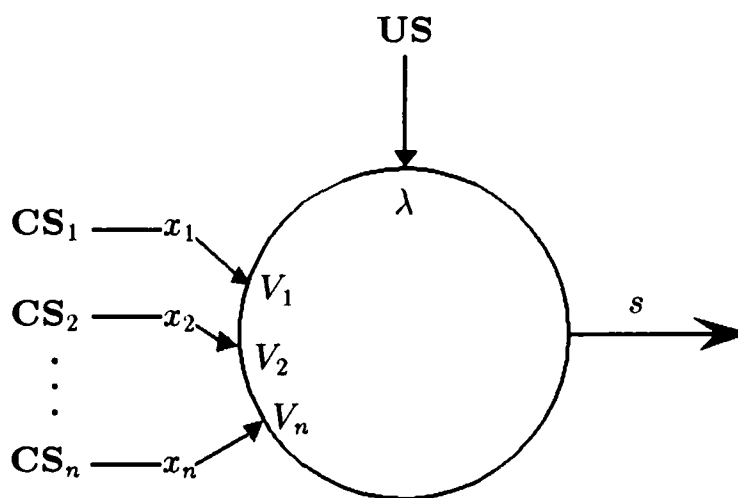
2

Figure 1. The Sutton and Barto neuron-like adaptive element. The unconditioned stimulus (US) is signaled by a pathway of fixed efficacy, denoted as λ. Inputs for each conditioned stimulus (CS) are denoted as x_i, i=1, ..., n, and vary in transmission efficacy according to the strength of a learned connection for each CS, the synaptic weight V_i. The output of the element, s, is computed as the weighted sum of all inputs.

activity of some types of neurons that have been identified in single-unit recording studies as being linked to the generation of CRs. For example, Desmond (1985; see also Desmond and Moore, 1986) described the activity of brain stem neurons recorded during classical conditioning of the rabbit NMR with a 350 ms tone CS (ISI of 350 ms). In a typical cell, spikes began to be recruited about 70 ms after CS onset. About 150 ms after CS onset, spike recruitment increased sharply and continued to increase throughout the remainder of the ISI. The momentary rate of firing prior to the US rarely exceeded 200-Hz. After US offset, firing initiated by the US declined toward a baseline rate of about 10-Hz.

The finding that the firing pattern of these brain stem neurons mirrored and preceded the behavioral CR as observed at the periphery provides some justification for shaping CR topography in the SB model by manipulating the input trace rather than imposing an arbitrary transformation on the element's output to achieve the desired CR topography. In essence, the current implementation of the SB model provides the element with a template of the CR.

We were able to fashion a suitable CR template by using an expression for CS input to the learning element that allows for variation in the recruitment and amplitude of the CR within the ISI. The input to the learning element at time t is denoted $x_i(t)$. Each time step t corresponds to 10 ms. At CS_i onset, $t = 0$. For time steps $t = 1, ..., 7$, $x_i = 0$. For

3

$t > 7$ and until CS_i offset, x_i is defined as follows:

$$x_i(t) = [arctan(mt - 5.5) + 90]/180\,h. \tag{1}$$

The parameter m, $m > 0$, controls the rate of rise of x_i, and the parameter h, $h > 0$, controls CR amplitude. The simulation experiments reported by Moore et al (1986) used $m = 0.35$ and $h = 1.0$. These are the default values of the model.

Holding $x_i = 0$ for the first 7 time steps precludes any changes in V_i during this period and aligns the model with reports indicating a minimal conditionable ISI of 70 ms for rabbits (Salafia, Lambert, Host, Chiaia, and Ramirez, 1980). It also precludes detectable CRs with latencies less than 70 ms.

A second function returns the CR generated by x_i to its pretrial baseline. It is implemented at CS_i offset, decays geometrically, and is computed as follows:

$$x_i(t + 1) = kx_i(t), \tag{2}$$

where $0 < k < 1$. In Moore et al (1986) $k = 0.85$, its default value in the model.

With the default values of the parameters of Equations 1 and 2, the model simulates features of the conditioned NMR: increasing amplitude and decreasing latency of the CR over training, decreasing amplitude and increasing latency of the response during extinction, and attainment of peak CR amplitude at the temporal locus of the US. These features are depicted in Figure 2. The variable s' on the ordinates of the panels of Figure 2 is a sliding mean over three time steps (the current and two preceding) of the element's output, s (defined below in Equation 4). s' is bounded between 0.1 and 1.0 as in our previous reports. The lower bound of 0.1 imposed on s' reflects a threshold due to recruitment effects between the model's output and the motoneurons which generate the peripherally observed response.

Learning Rule

The equation dictating changes in synaptic weight (connection strength) is retained from the original SB model. At time t, the the change in synaptic weight of CS_i, denoted as ΔV_i, is computed as follows:

$$\Delta V_i(t) = c[s(t) - \bar{s}(t)]\bar{x}_i(t), \tag{3}$$

where c is a learning rate parameter, $0 < c \leq 1$, $s(t)$ is the element's output at time step t, and $\bar{s}(t)$, defined below, is a function of $s(t)$ from preceding time steps. $\bar{x}_i(t)$, the eligibility of CS_i, is defined below.

4

ACQUISITION

EXTINCTION

Trial 1 · Trial 1

Trial 2 · Trial 2

Trial 5 · Trial 10

Trial 25 · Trial 25

CS US · CS CS
On On · On Off
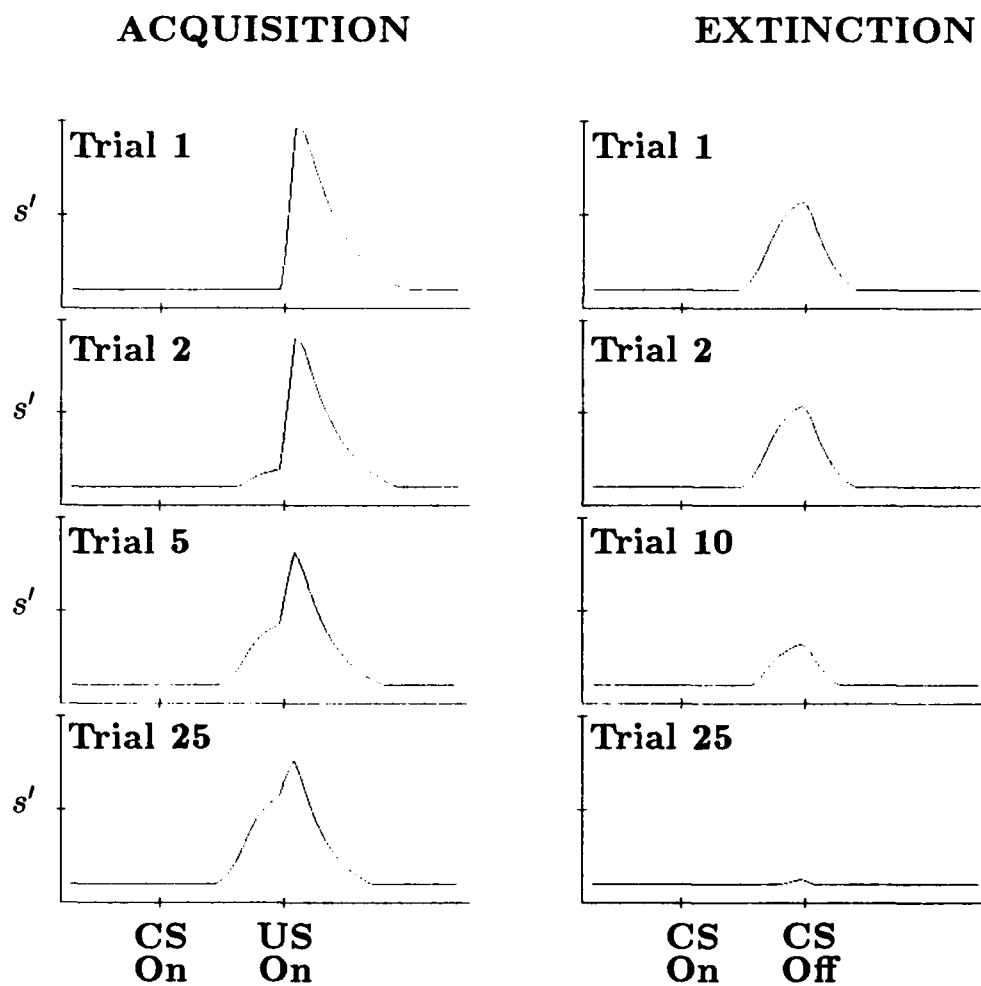
Figure 2. Simulated response topographies, s', obtained with a 250 ms ISI during acquisition and extinction in a forward-delay paradigm. The US duration = 30 ms. The data were generated with the following parameter values: $m = 0.35$, $h = 1.0$, $k = 0.85$, λ, $= 0.9$; $c = 0.15$, and $\beta = 0.6$. In this and subsequent figures depicting response topography, s' is a sliding mean of the element's output, s, over three time steps, the current one and the two preceding, bounded between 0.1 and 1.0.

5

Output

The output of the learning element at time t, denoted $s(t)$, is defined as:

$$s(t) = \sum_{i=1}^{n} V_i(t) x_i(t) + \lambda'(t). \tag{4}$$

$\lambda'(t)$ is defined below. While s can take on any real value in the SB model, in the SBD model it is confined to the closed unit interval and is linear within that range. This limitation on permissible values of s is imposed because of physiological constraints of the NMR: Negative values of s are inappropriate in modeling NMR topography because they imply NM retraction and exopthalmus, CR-opposing responses which are not typically observed in the rabbit. The upper bound of 1.0 reflects the fact that, although the amplitude of the NMR is directly related to the intensity of the eliciting stimulus, there are limits on the number of involved motoneurons and their rate of firing (Berthier and Moore, 1980; Moore and Desmond, 1982).

Variable $\lambda'(t)$ in Equation 4 equals 0 prior to the occurrence of the US. During US presentation λ' is calculated as the difference between λ, the weight of the US, and the largest positive starting weight among all CSs present on a given trial. (Starting weight refers to the weight of a given CS at $t = 0$.) Thus, if V_i is the largest starting weight among the CSs present on the trial, while the US is present

$$\lambda' = \begin{cases} \lambda - V_i & \text{if } 0 \leq V_i \leq \lambda; \\ 0 & \text{if } V_i > \lambda; \\ \lambda & \text{if } V_i \leq 0. \end{cases} \tag{5}$$

At US offset, λ' decreases as follows:

$$\lambda'(t+1) = 0.9\lambda'(t). \tag{6}$$

Although λ in the model is a constant directly related to US intensity, λ' functions as a heuristic that implements the idea that US effectiveness can diminish progressively with training (e.g., Donegan and Wagner, 1987; Mackintosh, 1983). Thus, in the SBD model the effectiveness of a US on a given trial is the difference between the amount of learning that can be supported in the limit by the US and the amount of learning accumulated up to that point in training. Because V_i generally increases during training, λ' progressively decreases, and this can induce a corresponding decrease in response amplitude at the time the US is presented. Figure 2 illustrates a progressive diminution of the unconditioned response (UR) over acquisition trials due to the progressively smaller contribution of $\lambda'(t)$

6

to $s(t)$ in Equation 4. (In this report, the UR is defined as the response profile during time steps containing the US).

Were $\lambda'(t)$ to be replaced in Equation 4 by λ, post-US computations would cancel increments in V_i during time steps preceding US offset, and as a result there would be no net learning (see Moore et al, 1986). In addition, response topography would be compromised.

Predicted Output

The trace of s, denoted $\bar{s}$, is computed by:

$$\bar{s}(t+1) = \beta\bar{s}(t) + (1-\beta)s(t),\tag{7}$$

where $0 \leq \beta < 1$. The parameter β determines the rate of decay of $\bar{s}$. $\bar{s}$ can be interpreted as the element's prediction or expectation of its output during the current time step.

Learning Eligibility

Variable $\bar{x}_i(t)$ in Equation 3 is a duration-dependent stimulus trace that defines the period and extent to which the ith synapse or connection is eligible for modification. For a given time step t, this *eligibility trace* is defined as follows:

$$\bar{x}_i(t) = x_i(t-4),\tag{8}$$

during time steps t that the CS_i is on. $\bar{x}_i$ begins its decline four time steps after CS_i offset:

$$\bar{x}_i(t+1) = \delta\bar{x}_i(t),\tag{9}$$

where $\delta = e^{-3/d}$, $d = \max\{25, CS_i$ duration in units of 10-ms$\}$. The computations shown define a period of eligibility which begins some time after CS_i onset and persists beyond CS_i offset. In earlier descriptions of the model (e.g., Moore et al, 1986), the lag between x and $\bar{x}$ was erroneously stated to be 3 time steps, or 30 ms. However, the computer code generating the SBD simulator computes $\bar{x}(t)$ as specified above in Equation 8, effectively producing a lag of 4 time steps or 40 ms. The simulation experiments presented in this report utilize a lag of 4 time steps as in Moore et al (1986).

Purpose and General Method

Because our simulation experiments in this report are limited to single-CS forward-delay paradigms, we henceforth suppress subscripts designating different CSs for the variables V_i, x_i, and $\bar{x}_i$.

We examined the sensitivity of the model to parameters of the input trace as specified in Equations 1 and 2. The values of other parameters of the model were the same as in previous reports (e.g., Moore et al, 1986). The learning rate parameter, c in Equation 3, was 0.15. The weight of the US, λ in Equation 5, was 0.9 in all experiments, and β, the output rate parameter in Equation 7, equaled 0.6. In all experiments, simulated training was in a forward-delay paradigm in which US onset occurred simultaneously with CS offset. The duration of the US was 30 ms. All simulations of training assumed that $V = 0$ prior to training.

In Experiment 1 we varied x-shaping parameters m, h, and k one at a time while holding the others constant at their default values. In Experiment 2 we investigated combinations of x-shaping parameter values. One of our goals was to determine the region of the parameter space in which the SBD model successfully simulates response topography as well as other aspects of NMR conditioning. A second goal was to determine whether some combination of x-shaping parameters might mitigate some of the shortcomings of the SBD model noted in our previous reports. For example, CR latency predicted by the model is too short to be realistic in protocols involving long ISIs (Smith, Coleman, and Gormezano, 1969). Also, the model predicts a negatively-accelerated learning curve instead of the S-shaped learning curve typically observed in the laboratory. In trace conditioning, the model also fails to appropriately place CRs within the trace interval (i.e., the interval between CS offset and US onset). It was recognized at the outset that no combination of x-shaping parameters would alleviate all problems with the model, but we hoped to uncover approaches to their solution.

We also examined the model's sensitivity to parameters of the learning rule (Equation 5) with reference to descriptions of learning curves, ISI effects, and response topography. These considerations provided a basis for discussion of a neural circuit implementation of components of the model. Several laboratories have demonstrated that learning and generation of conditioned NMRs involves the cerebellum, particularly hemispheral lobule VI (HVI) (Berthier and Moore, 1986; Yeo, Hardiman, and Glickstein, 1984, 1985a-c, 1986). In the Discussion, we consider various schemes by which the cerebellar circuits might be aligned with modification of synaptic weight as specified by the SBD model.

Experiment 1: Variation of x-shaping Parameters

Experiment 1 investigated parameter sensitivity of the model. In Experiment 1, one parameter of x was varied at a time while other parameters were held constant at their default values. We looked for evidence that certain parameter values might mitigate prob-

lems in the behavior of the SBD model mentioned previously: failure to predict longer CR latency in long-ISI forward-delay paradigms and the failure to predict S-shaped learning curves. We assessed the effects of each parameter value on acquisition and CR topography for ISIs of 100, 250, 350, 500, and 700 ms. We examined six values of m (0.1, 0.2, 0.35, 0.6, 0.8, and 1.0), five values of h (0.25, 0.5, 0.75, 1.0, and 2.0), and seven values of k (0.0, 0.1, 0.25, 0.45, 0.65, 0.85, and 1.0). Notice that with $k = 1.0$, x can not return to pretrial baseline (Equation 2). $k = 1.0$ is included to provide a contrast with permissible values of k.

Learning Curves: Shape and Rate of Acquisition

Manipulation of m

Figure 3 shows the acquisition of V generated over 25 training trials under variation of m. This and subsequent figures in which V is the dependent variable refer to values of V as they exist during static periods, i.e., during intertrial epochs when x and $\bar{x}$ are essentially 0. V is dynamic during CS presentations and for a period thereafter, tending to rise from its intertrial level as the output of the learning element, s, increases and falling back to some extent as s declines. This occurs because V can change only when $\bar{x}$ exceeds 0: $\bar{x}$ increases during the ISI, up to and including the time of US occurrence, and declines during post-US epochs.

Figure 3 shows that when $m = 0.35$, V grows in a negatively-accelerated fashion to a value of 0.59 in about 15 trials. Values of m greater than 0.35 (i.e., 0.6, 0.8) do not appreciably alter rate of acquisition or maximum value of V. Low values of m (e.g., 0.1 and 0.2) yield slow acquisition. With $m = 0.1$, the model requires 700 trials to attain a stable value of 0.88. This is considerably higher than the terminal weight of 0.59 attained much more quickly with $m = 0.35$.

Acquisition with $m = 0.1$-0.2 is slow because the value of x is low throughout the ISI. As implied by Equation 4, the element's output is directly influenced by the magnitude of x. The slow rise of x during the ISI results in a low value of $s(t) - \bar{s}(t)$ in Equation 3. Furthermore, $\bar{x}$, which defines the time and extent to which V can be modified, is also small during this period. Thus, V grows in minute increments over acquisition trials.

Figure 4A shows values of V obtained after 50 trials as a function of m. This figure indicates that V increases as m increases from 0.1 to 0.35 and decreases for $m > 0.35$. V is smaller when $m = 0.6$-1.0 than when $m = 0.35$ because the value of x is nearly 1 in the eighth time step after CS onset. (Recall that according to the assumption of a
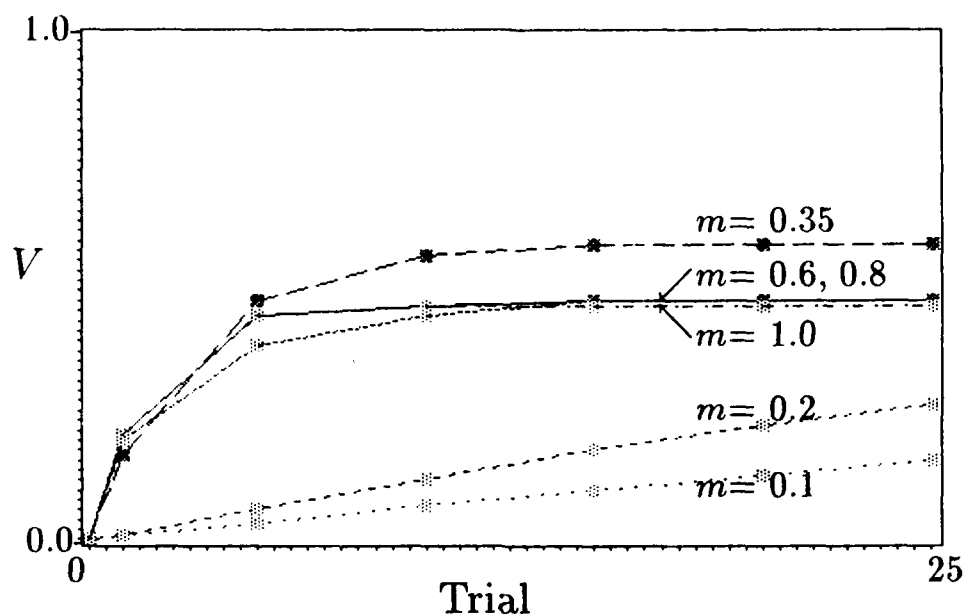
9

Figure 3. Acquisition of V with a 250 ms CS paired with a 30 ms US at an ISI of 250 ms with various values of m.

minimum conditionable ISI, $x = 0.0$ during the first 7 time steps). Since x is practically at its maximum before $\bar{x}$ exceeds 0, $s - \bar{s}$ is on the order of 0.01 on the eighth time step. Given such a value of $s - \bar{s}$, increases in V are negligible.

Manipulation of h

Figure 5 shows acquisition of V under variation of h. When $h = 1$, the default value, the learning curve is negatively-accelerated and stabilizes in about 15 trials. The most rapid acquisition occurs when h is low, e.g., $h = 0.25$, and the slowest rate of acquisition is obtained when $h = 2.0$. Figure 4B plots terminal values of V as a function of h. The figure shows that V is a minimum in the neighborhood of $h = 1$, the default value; the maximum is at $h = 0.25$. Within a range of values from 0.5 to 1.0, rates of acquisition are about the same (Figure 5), and V values after 50 trials (Figure 4B) are approximately equal.

Taken together, Figures 4B and 5 indicate that a low value of h such as 0.25 results in rapid learning and a high terminal weight. This result follows from Equations 1 and 5: When $h < 1.0$, the value of x is uniformly greater than the value of x obtained with $h \geq 1.0$. In addition to the larger value of x, with $h < 1.0$, $s - \bar{s}$ is large early in the ISI,
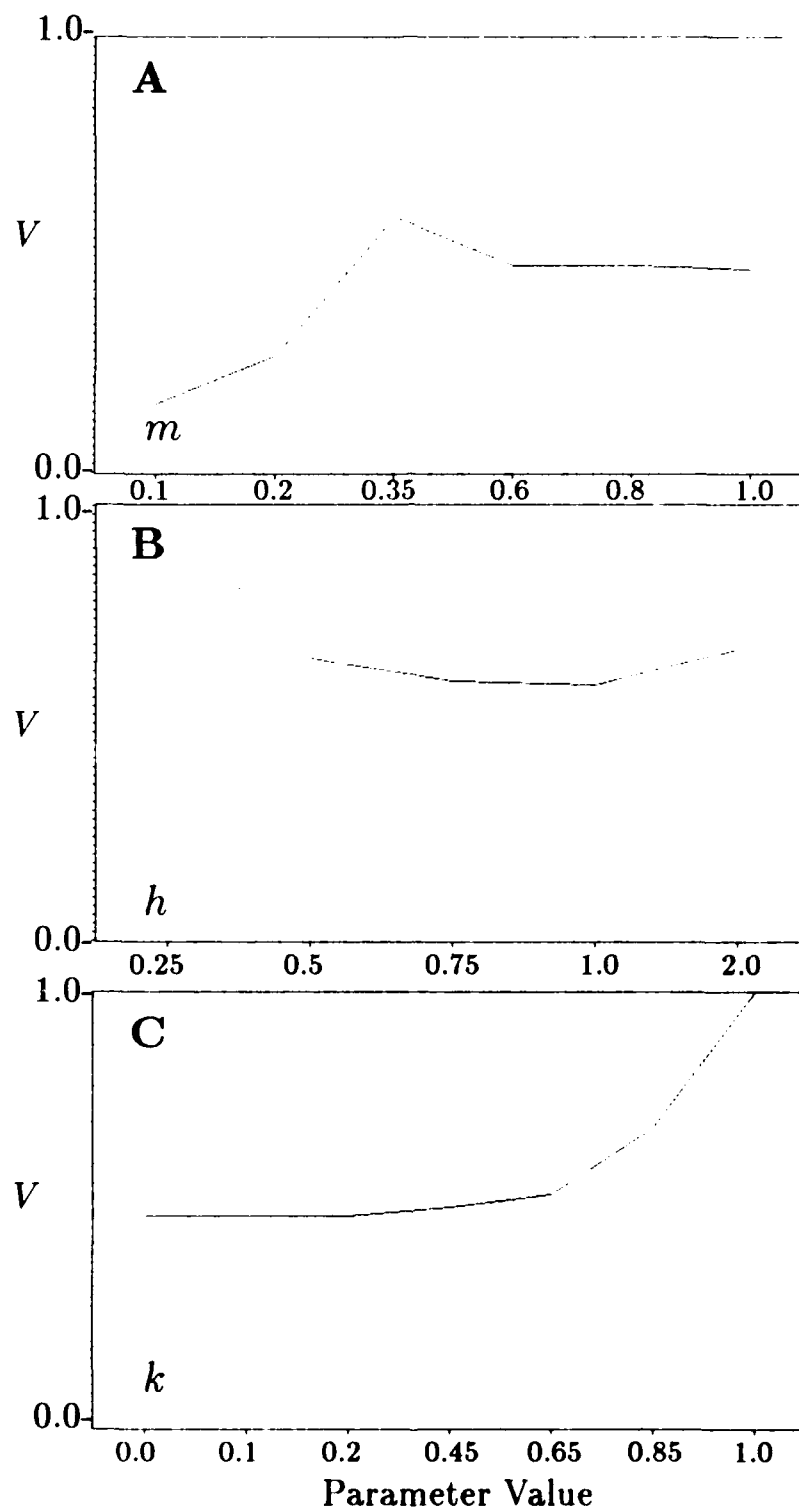
10

Figure 4. V obtained with a simulated 250 ms ISI in a forward-delay paradigm after 50 trials. Panel A shows the value of V obtained with various values of m. Panel B shows the value of V obtained as h is varied. Panel C depicts the value of V obtained with various values of k.
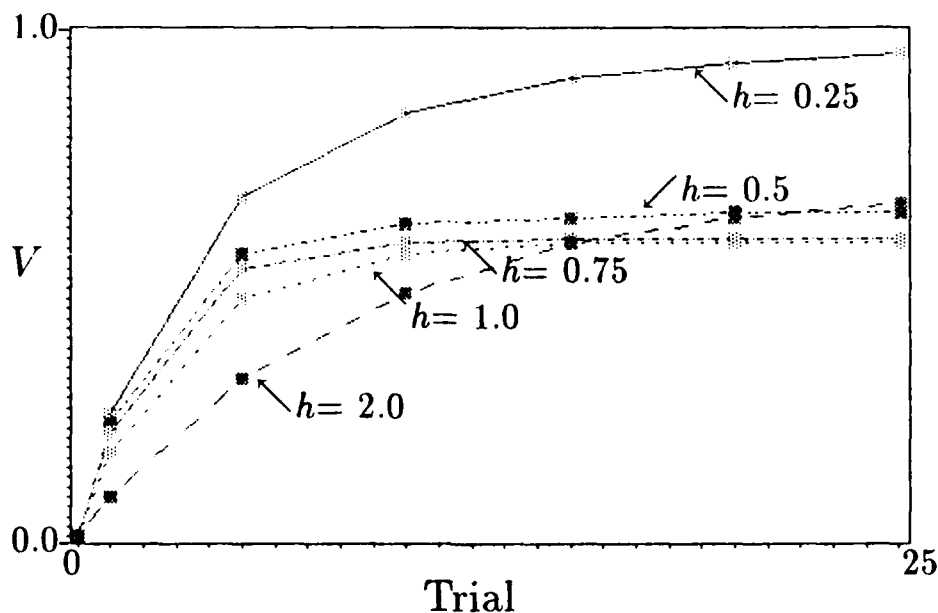
Figure 5. Acquisition of V with a 250 ms CS paired with a 30 ms US at an ISI of 250 ms with various values of h.

giving larger-than-average increments in V. This accounts for the observation that rate of acquisition and terminal value of V increase as h decreases below 1.0.

Although $h = 2.0$ produces much slower arquisition than $h = 1.0$ (Figure 5), the terminal value of V is slightly greater with $h = 2.0$ than with $h = 1.0$ (Figure 4B). The slow rate of acquisition with $h = 2.0$ is due to the fact that x and $\bar{x}$ are low throughout the ISI, resulting in a low value of $s - \bar{s}$ during this period. However, at US onset, $s - \bar{s}$ is large enough to compensate for low values of x and $\bar{x}$, and eventually terminal values of V exceed those obtained with the default value.

Manipulation of k

Figure 6 shows that all values of $k < 1.0$ yield negatively-accelerated learning curves. Both the rate of acquisition and terminal weight are directly related to this parameter. As shown in Figure 4C, V after 50 trials is an increasing function of k, increasing slowly through the range $0 \leq k \leq 0.65$ and increasing rapidly up to $k = 1.0$. When $k = 1$, x does not decay at CS offset and consequently V accumulated during the ISI and presentation of the US does not undergo the post-trial reduction that would otherwise result from negative values of $s - \bar{s}$ during the period of declining eligibility. Moreover, extinction does not occur
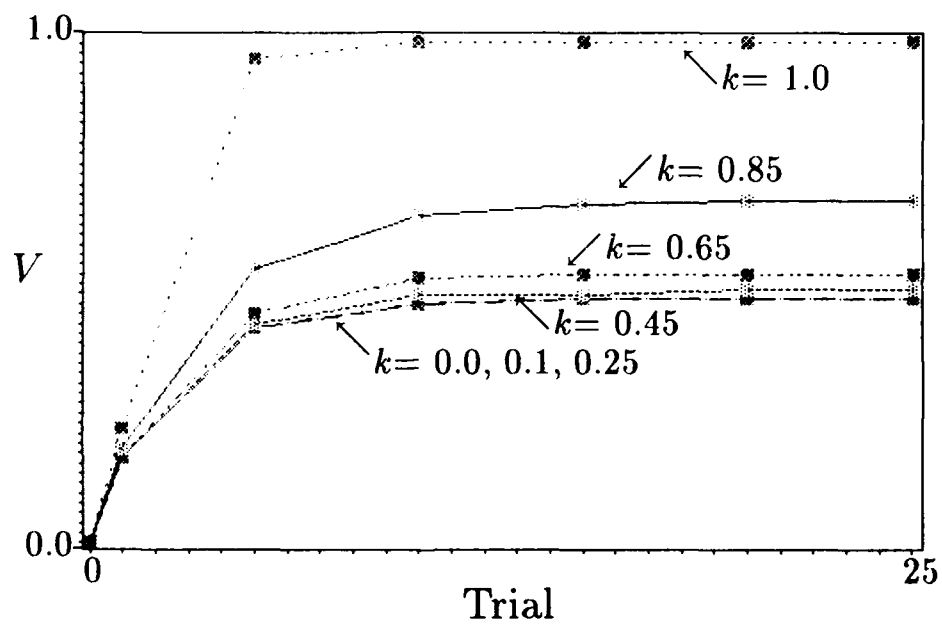
12

Figure 6. Acquisition of V with a 250 ms CS paired with a 30 ms US at an ISI of 250 ms with various values of k. When $k = 1.0$, V exceeds 1.0 within 10 trials and reaches 3.5 within 25 trials.

when $k = 1.0$.

Response Topography

As mentioned in the Introduction, NMR topography has the following features. The CR rises gradually in a ramped or S-shaped fashion after CS onset to a peak amplitude at or near the time of the US. The response decays rapidly after US offset. Response profiles generated by the model under variations in the values of h, m, and k were assessed against these criteria. Thus, simulated responses that are square-shaped or that do not maintain a smooth, continuous rate of increase over the ISI are not realistic. There are exceptions to this characterization, of course, but it is generally applicable to forward-delay and trace paradigms with ISIs less than 1 sec.

Manipulation of m

With $m = 0.35$, the default value, the model produces the realistic responses depicted in Figure 2. No other value of m examined here works as well. Figure 7 shows two simulated responses; one generated with $m = 0.1$ (Figure 7A) and the other with $m = 0.6$ (Figure 7B). Because m affects rate of learning, and since we wish to contrast response topographies with V held constant, Figures 7A is based on a greater number of trials (100) than Figure 7B (25). Figure 7A shows that with $m = 0.1$ and an ISI of 250 ms, a detectable CR does not appear within 100 trials. This is the case with any value of $m \leq 0.2$. The failure to develop a CR arises from the very low amplitude of x; for example. with $m = 0.1$ the peak value of x computed with an ISI of 250 ms is less than 0.04.

Low values of m not only tend to preclude detectable CRs. they exaggerate the decline of UR amplitude over training trials implied by Equations 4 and 5. Given enough training, the UR disappears altogether with $m \leq 0.2$. For example, with $m = 0.1$, s after 700 trials is only 0.15 at the time of US onset. This value of $s(t)$ follows from Equation 4 because even though $V = 0.88$ at US onset, $x = 0.03$. Thus, s barely surpasses the predefined threshold of 0.1 for s'. This loss of UR amplitude emphasizes an interesting feature of the model: Given enough training, V can attain a high value, but this does not necessarily imply the occurrence of detectable CRs.

Since m influences the rate at which x increases, higher values of m yield CRs that rise rapidly early in the ISI. The CR obtained with $m = 0.6$ in Figure 7B not only rises quickly, it abruptly changes slope midway through the ISI. The latter portion of the CR is relatively flat until US onset. The inappropriately short CR latency and abrupt change of slope are not typical of real conditioned NMRs. Only values of m in the neighborhood
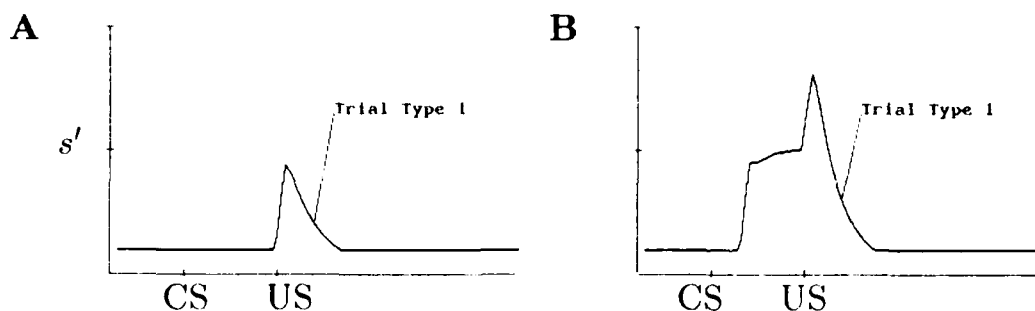
Figure 7. Simulated response topographies with a 250 ms ISI in a forward-delay paradigm after 100 trials in A and 25 trials in B. The hash marks on the abscissae designate stimulus onset. In A, $m = 0.1$ and $V = 0.48$ at the start of the trial. In B, $m = 0.6$ and $V = 0.48$ at the start of the trial.

of 0.35 maintain a smooth, continuous topography and appropriate rates of acquisition.

Figure 7 illustrates that the value of m not only affects CR amplitude, but also UR amplitude. The difference in UR amplitude is not a consequence of different values of λ', because V is equal for the two response profiles depicted in Figure 7. Instead, the difference in UR amplitude reflects different values of x during US time steps. Although the simulation assumed that the US occurred at CS offset, x nevertheless contributes heavily to s' during US epochs. In Figure 7A, x is quite low at US offset; in Figure 7B, x at the time of US onset is nearly ten times higher than in 7A, resulting in a greater UR amplitude.

Manipulation of h

The effects of h on NMR topography are illustrated in Figure 8. The response simulated with $h = 1.0$, the default value, is shown in Figure 8C. Figure 8A shows that the CR produced with $h = 0.25$ rises quickly within the ISI and is soon clipped by the imposed ceiling of 1.0 on s'. These inappropriately clipped CRs occur with any values of $h \leq 0.5$. Simulated CRs with $h > 0.5$ generally appeared realistic, most notably in a decreased disparity between peak amplitude of the CR and the amplitude of UR. Figures 8B and 8C indicate that blending of the CR into the UR is somewhat better with $h = 0.75$ than with $h = 1.0$. The improved blending of CR into UR occurs because x attains a greater amplitude when $h = 0.75$ than when $h = 1.0$. With the 250 ms ISI used in Figure 8, x is nearly 1.0 at US onset when $h = 0.75$ and 0.95 when $h = 1.0$. Figure 8D shows that UR amplitude with $h = 2.0$ is lower than with other values of h. This reduction occurs for the
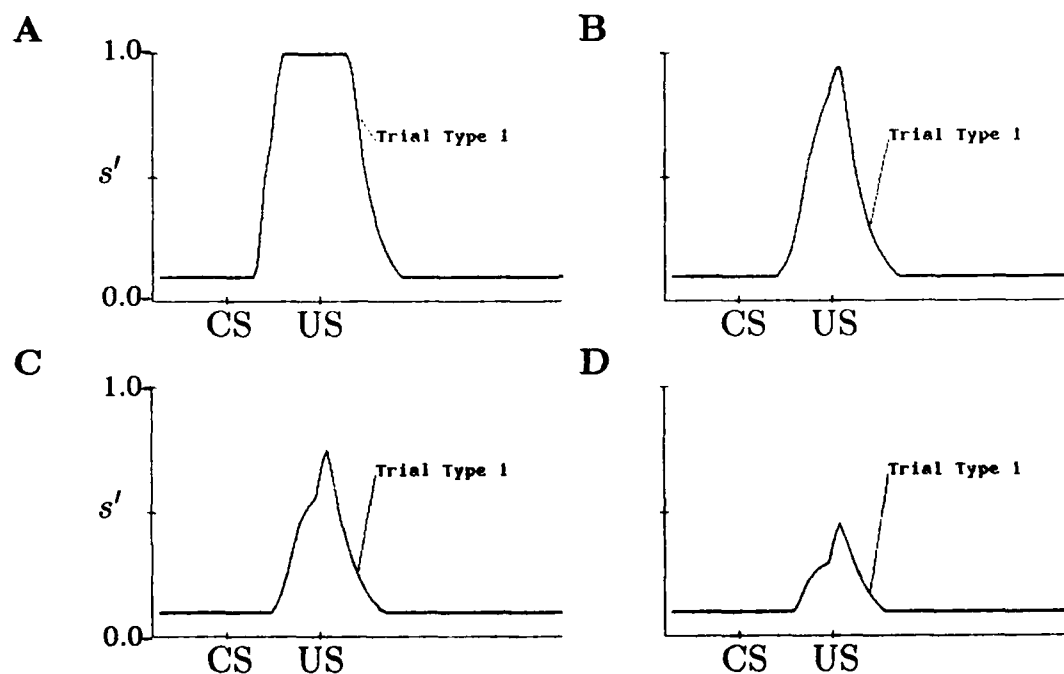
15

Figure 8. Simulated response topographies obtained with a 250 ms ISI in a forward-delay paradigm after 25 trials. In A, $h = 0.25$. In B, $h = 0.75$. In C, $h = 1.0$ (the default value for h in the current implementation). In D, $h = 2.0$.

same reasons as we noted in connection with Figure 7. In Figure 8D x is one-half as large at the time of the US as in 8C in which $h = 1.0$.

Manipulation of k

Figure 9 shows that parameter k affects the profile of the post-CS response. The figure depicts response profiles on trials in which Vs were about the same, i.e., after 10 reinforced trials in Figure 9A, 5 reinforced trials in Figure 9B. Figures 9A and 9B, in which $k = 0.25$ and 0.85 (the default value), respectively, show the effect of k on UR amplitude. Figure 9A shows that the lower value of k results in a lower UR amplitude. This lower UR amplitude in 9A is due to rapid decay of x at CS offset: With $k = 0.25$, x in the time step after CS offset is 0.22; with $k = 0.85$, x in this time step is 0.86.

The response profiles in Figures 9C and 9D are obtained after one extinction trial. Figures 9C and 9D, in which $k = 0.25$ and 0.85 respectively, illustrate the point that the decline of x decreases as k increases. The sharp drop in CR amplitude at CS offset with $k = 0.25$ in Figure 9C is not realistic. This effect of k is obscured in Figures 9A and 9B by the decay of λ' (Equation 6).

Interstimulus Interval Effects

Interstimulus interval (ISI) functions typically plot some measure of conditioning strength after an arbitrary number of trials as a function of the ISI used during training. ISI functions are typically concave downward. The rabbit NMR literature describes the ISI function as an inverted U that rises sharply from the minimal ISI that can support conditioning, approximately 100 ms, to a peak at the optimal ISI of 250 ms. The function declines gradually as ISI increases beyond the optimal range such that little or no learning occurs at ISIs greater than 2000 ms (Gormezano et al, 1983).

The default values of the SBD model produce an ISI function generally consistent with the literature, with the exception of negative weights predicted for CSs of 100 ms duration (the shortest considered) with a 40 ms lag between x and $\bar{x}$. In the context of the SBD model, negative values of V are interpreted as inhibitory, and there is no evidence to support this in the experimental literature.

Figure 10 shows ISI functions for each set of parameter values. With the exception of negative weights at ISI 100 ms, Figure 10 shows that most values of m and k, and all values of h, yield realistic ISI functions. However, with $m = 1.0$ (Figure 10A), the ISI function is inappropriate because V increases uniformly as ISI increases. With $m = 0.1$,
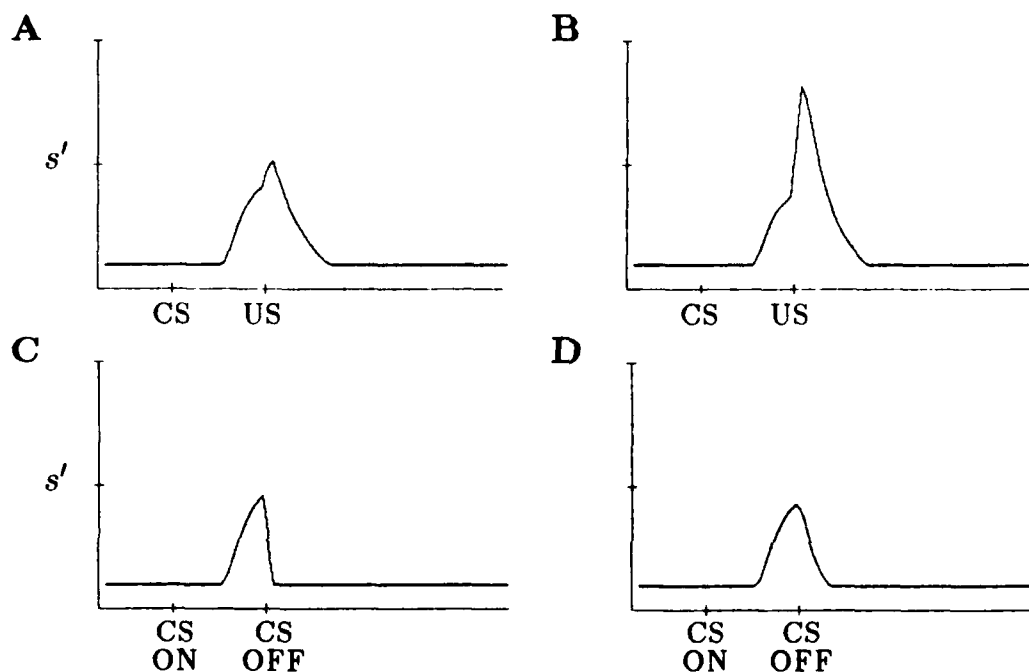
Figure 9. Simulated response topographies with a 250 ms ISI in the forward-delay paradigm; $V = 0.44$ at the start of each depicted trial. In A, there were 10 prior training trials, the CS is followed by the US, and $k = 0.25$. In B, there were 5 prior training trials, the CS is followed by the US, and $k = 0.85$. In C, there were 10 prior training trials, the CS is not followed by the US, and $k = 0.25$. In D, there were 5 prior training trials, the CS is not followed by the US, and $k = 0.85$.

18

Figure 10. Synaptic weight V after 100 trials as a function of interstimulus interval (ISI) in the forward-delay paradigm. In A, ISI functions with m ranging from 0.1 to 1.0. The asterisk (*) marks the function with $m = 0.1$. In B, ISI functions with h ranging from 0.25 to 2.0. In C, ISI functions with k ranging from 0 to 1.0. See text for discussion of $k = 1.0$.

19

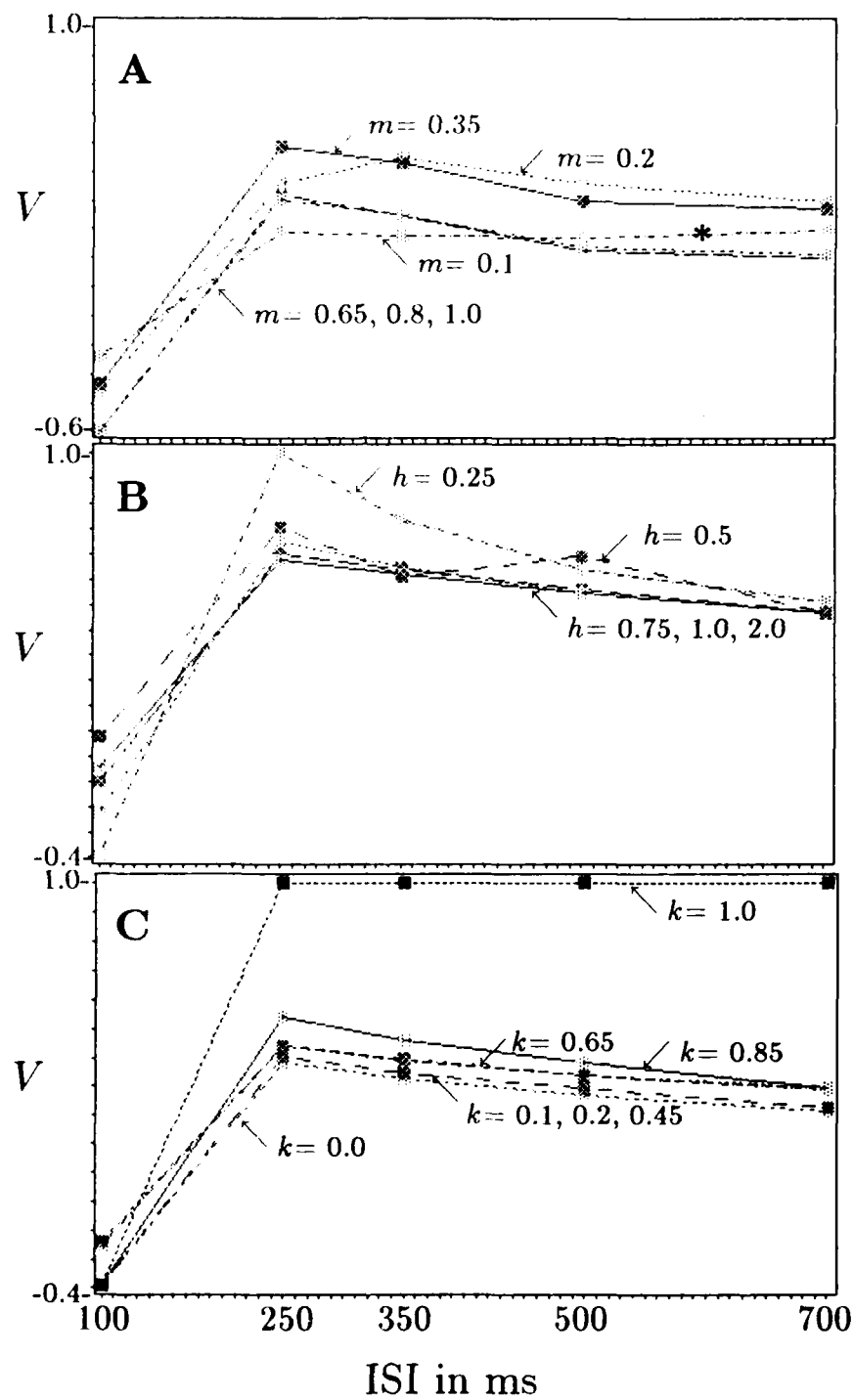ISIs greater than the optimum promote greater terminal values of V because low values of m allow x, and therefore $s - \bar{s}$, to be positive throughout the ISI. Longer ISIs provide more opportunities for V to increase. In Figure 10C, $k = 1.0$ yields an inappropriate ISI function: $V = 3.5$ (plotted as 1.0 because of compression of the ordinate) for all ISIs greater than 100 ms. The ISI function predicted for $k = 1.0$ is flat for most ISIs and is therefore inconsistent with the literature.

Experiment 2: Combinations of x-shaping Parameters

Experiment 2 investigated combinations of x-shaping parameter values, m, h, and k. We selected values of each parameter that appeared on the basis of Experiment 1 to have a noticeable effect on the model's behavior. For comparison purposes, all simulations included the default set. In Experiment 2, four values of h (0.25, 0.75, 1.0, 2.0), three values of k (0.25, 0.65, 0.85), and three values of m (0.1, 0.35, 0.7) were covaried orthogonally. We assessed the effects of covariations of parameters on rates of learning and response topography for ISIs of 250 and 600 ms.

Learning Curves: Shape and Rate of Acquisition

Figures 11 and 12 plot V as a function of trials for the various combinations of m and h with $k = 0.85$. Figure 11 was generated with an ISI of 250 ms; Figure 12 was generated with a 600 ms ISI. Most learning curves are similar to that produced with the default combination in that V is a negatively-accelerated function of trials. Rate of acquisition is uniformly low with $m = 0.1$, as might be expected from Figure 3, and in fact most of the data plotted in Figures 11 and 12 might have be inferred from Experiment 1.

Figures 11 and 12 show that no parameter combination yields an S-shaped learning curve. As presently formulated, the SBD model assumes that the form of the input trace x is invariant over trials, an assumption which may reflect neurobiological reality. It is possible that an S-shaped learning curve might be obtained from the model by using more than one parameter combination to shape the input trace over training. We discuss the implications of varying the form of x in later sections.

Figure 13 plots V after 50 trials for ISIs of 250 and 600 ms for the combinations of m and h plotted in Figures 11 and 12. Thus, Figure 13 is a plot of the terminal values of V shown in these two figures. As might be inferred from those figures, with combinations of m

Figure 11. Acquisition of V with an ISI of 250 ms in a forward-delay paradigm; values of parameters m and h are covaried and $k = 0.85$. In A, $h = 0.25$. In B, $h = 0.75$. In C, $h = 1.0$. In D, $h = 2.0$.
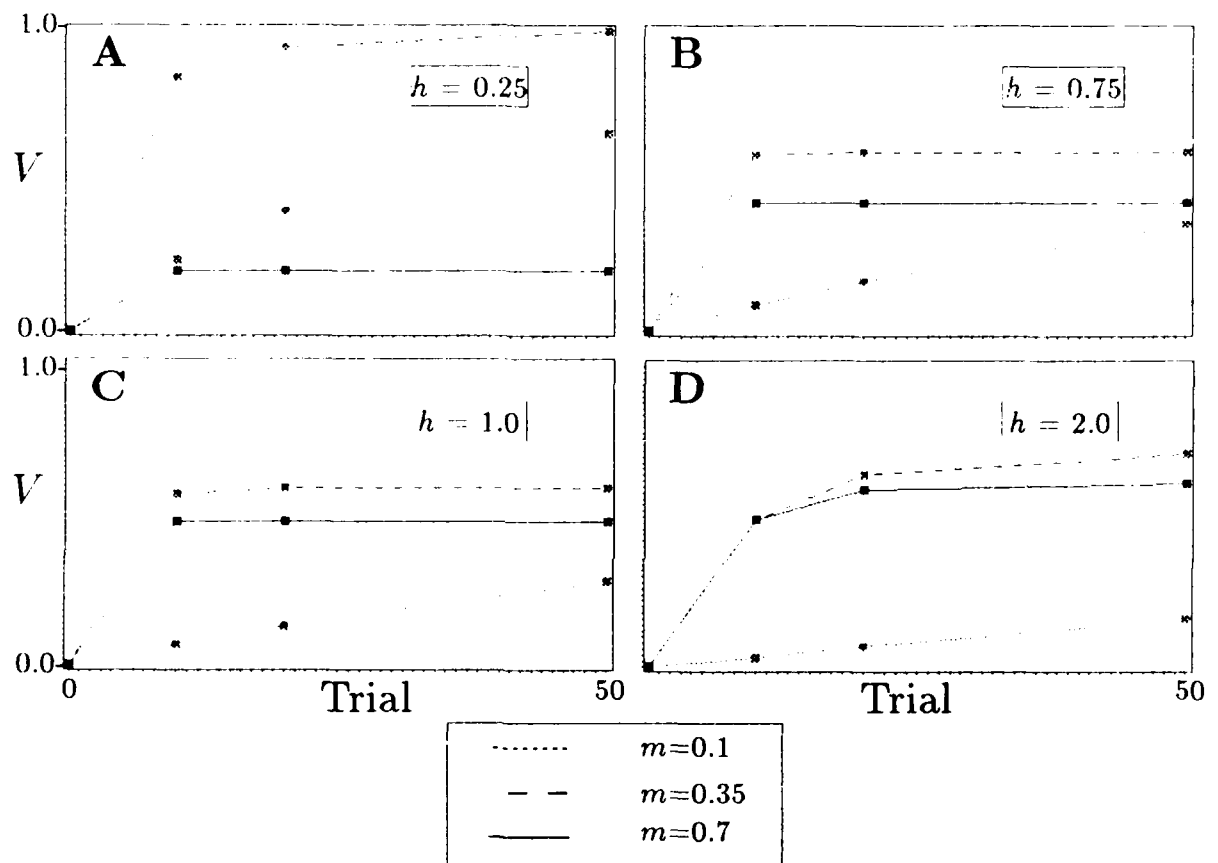
21

Figure 12. Acquisition of V with an ISI of 600 ms in a forward-delay paradigm; values of parameters m and h are covaried and $k = 0.85$. In A, $h = 0.25$. In B, $h = 0.75$. In C, $h = 1.0$. In D, $h = 2.0$.
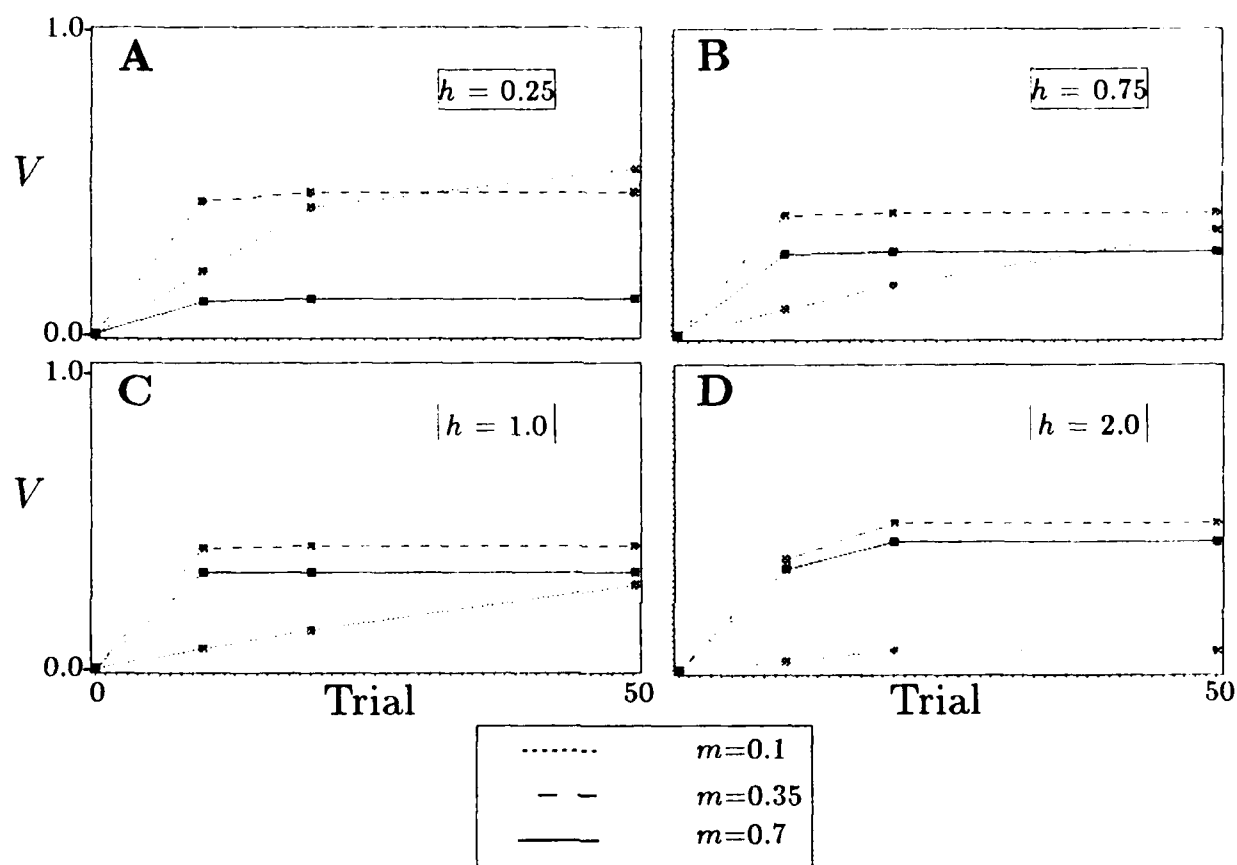
and h excepting those with $m = 0.1$, V with a 250 ms ISI (Figure 13A) is higher than with a 600 ms ISI (Figure 13B). Although not shown, this pattern also holds with $k = 0.25$ and $k = 0.65$. (As might be inferred from Figure 4C, V is directly related to k for all parameter combinations.) Thus, ISI effects on V appear to be relatively insensitive to combinations of x-shaping parameters that depart from the default set, exceptions being those noted in connection with Experiment 1, low values of m and $k = 1.0$. However, although all other combinations tested yield appropriate ISI effects, they are not all suitable with respect to other criteria.

One noteworthy feature of Figure 13 is the low values of V obtained with the combination $m = 0.7$ and $h = 0.25$. Learning curves (Figures 11 and 12) indicate that these low values of V stabilize well before 50 trials. Low terminal values of V with this combination appear somewhat paradoxical because $m = 0.7$ leads to a reasonably high V when $h = 1.0$ (Figure 4A), as does $h = 0.25$ when $m = 0.35$ (Figure 4B). There is no paradox because a combination of high m and low h produces a rapid rise in x during the ISI. After a few trials, this drives s to the imposed ceiling of 1.0 (see Figure 8A) before $\bar{x}$ exceeds 0. Because of this ceiling, by the time $\bar{x}$ becomes significantly positive, $s - \bar{s}$ goes to 0, and consequently no further changes in V are possible.

Response Topography

Figure 14 illustrates response profiles with selected combinations of x-shaping parameter values with ISIs of 250 and 600 ms. The combination $m = 0.7$, $h = 0.25$, and $k = 0.25$ was used to generate Figures 14A and 14B. The combination $m = 0.7$, $h = 2.0$, and $k = 0.85$ was used to generate Figures 14C and Figure 14D. Response profiles in Figures 14A and 14C can be contrasted with that generated by the default set, $m = 0.35$, $h = 1.0$, and $k = 0.85$ (Figure 8C). The results depicted in Figure 14 suggest that response characteristics generated by a given parameter combination with the 250 ms ISI (Figures 14A and 14C) also hold for the longer ISI (Figures 14B and 14D). Combinations with $m = 0.7$ result in a response that rises rapidly but which then increase slowly over time steps leading up to the US. As noted in Experiment 1, $h = 0.25$ results in larger response amplitudes than those produced by the default set. These are, in turn, larger than those generated with $h = 2.0$. The influence of k on response profiles is obscured in Figure 14 by the contribution of λ' to responses shown in Figures 14C and 14D, but as noted previously k simply determines the decay of the response after CS offset. Although values of k used in Experiment 2 do not affect acquisition or ISI functions in any dramatic fashion, we know from Experiment 1 that low values of k yield undesirably low UR amplitudes and durations.

23
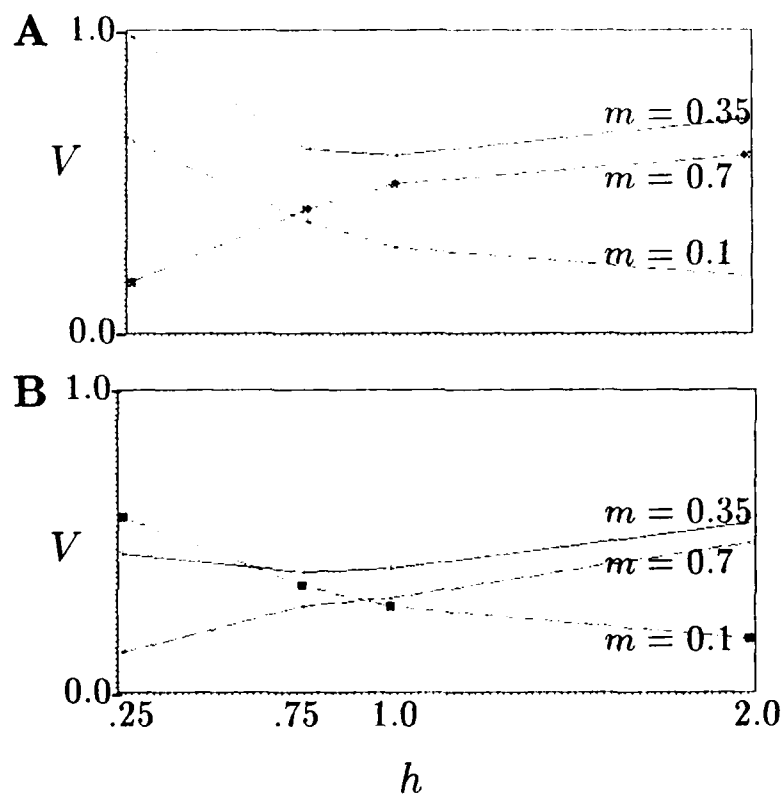
Figure 13. *V* obtained with ISIs of 250 and 600 ms in a forward-delay paradigm after 50 trials; values of *m* and *h* are covaried and *k* = 0.85. In Panel A, the ISI is 250 ms. In Panel B, the ISI is 600 ms.

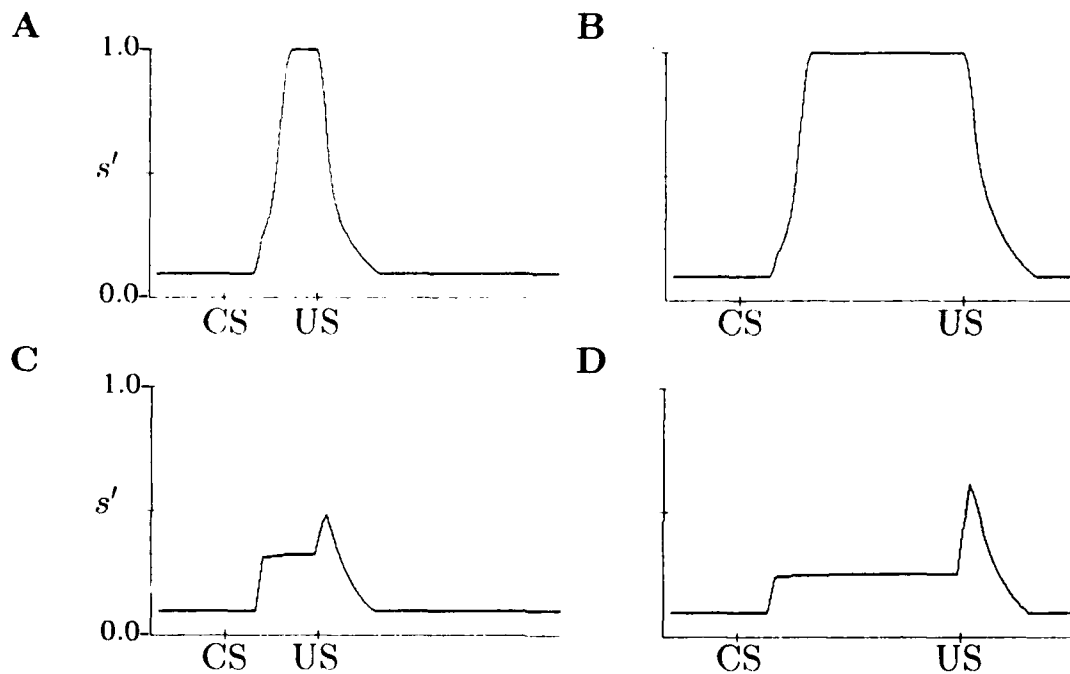**Figure 14.** Simulated response topographies with ISIs of 250 and 600 ms in a forward-delay paradigm after 25 trials. In A, $h = 0.25$, $m = 0.35$, and $k = 0.25$; the ISI is 250 ms. In B, the parameter combination of A is shown for a 600 ms ISI. In C, $h = 2.0$, $m = 0.7$, and $k = 0.85$; the ISI is 250 ms. In D, a 600 ms ISI is shown with the parameter combination used in C.
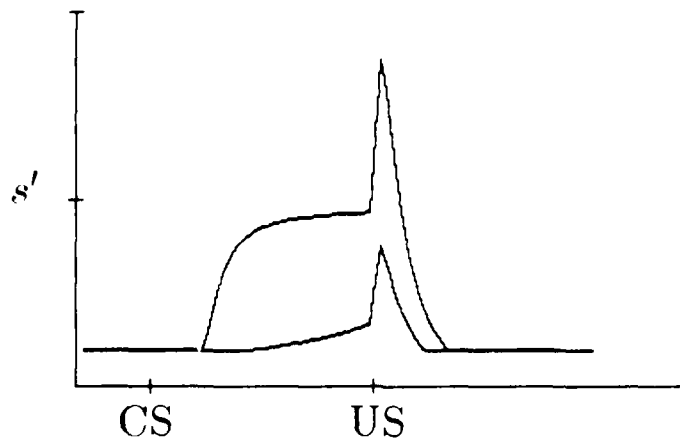
Figure 15. Simulated response topographies for a 600 ms ISI in a forward-delay paradigm after 50 trials. For the upper waveform, $m = 0.35$, $h = 1.0$, $k = 0.85$, and $V = 0.59$ at the start of the trial. The CR appears earlier in the ISI than is observed in the laboratory. For the lower waveform, $m = 0.1$, $h = 0.25$, $k = 0.85$, and $V = 0.66$ at the start of the trial. CR latency is appropriately longer, but response amplitude is attenuated.

Figure 15 addresses the issue of inhibition of delay with a long ISI. It contrasts response profiles generated after 50 trials with the default set with those generated with $m = 0.1$, $h = 0.25$; $k = 0.85$. With the default set the CR begins to rise early in the ISI and consequently does not show inhibition of delay. This is because s' with $m = 0.35$ and $h = 1.0$ surpasses the threshold of 0.1 450 ms before the US. However, with $m = 0.1$ and $h = 0.25$ s' does not exceed 0.1 until 260 ms before the US. (Therefore, there would be no detectable CR with an ISI of 250 ms.) The latency of the CR better reflects that observed in the laboratory. Moreover, the form of the CR in this case does not have the large amplitude and S-shaped form that are obtained with the default set.

Figure 15 shows that the UR obtained with the default set is substantially larger than that obtained with $m = 0.1$ and $h = 0.25$. With the default values, $x = 0.98$ and V is 0.70 at US onset, and λ' is 0.31. Therefore during the US s' is approximately 0.9. With $m = 0.1$ and $h = 0.25$, $x = 0.27$ and $V = 0.67$ at US onset, and $\lambda' = 0.24$. Therefore s' is approximately 0.4.

In summary, Experiment 2 shows that the parameter combination $m = 0.35$, $k = 0.85$, and $h = 0.75$-1.0 optimizes performance of the model with respect to acquisition, response topography at near-optimal ISIs, and appropriate ISI functions. With the 600 ms ISI, no combination appears to produce a CR with both the desired long latency and high

26

amplitude at US onset. Nor does any combination yield an S-shaped learning curve.

Discussion

Experiment 1 showed that when m 0.1 the CR fails to develop and the UR eventually disappears as training progresses. Values of m greater than the default value of 0.35 tend to yield CR topographies that abruptly change slope. Experiment 1 also showed that m is the only parameter of x that markedly affects ISI functions. When m 0.1, the SBD model predicts that terminal weights are an increasing function of ISI. Values of m larger than this yield an appropriate decline in V as ISI increases beyond an optimal of 250 ms. Parameter h ($h > 0$) affects CR amplitude and rate of learning. CR amplitude is inversely related to h. When h 0.75, the model produces a behaviorally realistic blending of the CR into the UR. Values of h ranging from 0.5 to 1.0 yield faster rates of acquisition than the more extreme values, h 0.25 or 2.0. Parameter k shapes response topography following CS offset, but beyond this has little affect on other aspects of the model's behavior except in the case where $k = 1$ in which CRs never return to pretrial baseline.

Experiment 2 investigated combinations of parameter values of x. One goal of Experiment 2 was to uncover a combination of parameter values that might produce inhibition of delay, i.e., increasing CR latency as ISI increases. The combination of h 0.25 and m 0.1 produces the desired increases in CR latency, but only at the cost of yielding an inappropriate ISI function in which V is an increasing function of ISI.

Sensitivity of the SBD Model to Other Parameters

With the exception of parameter h, Experiments 1 and 2 generally justified the choice of parameter values for x used in previously reported simulations with the SBD model: m 0.35, h 1.0 and k 0.85. As noted above, response topography is somewhat more realistic with h 0.75 than with h 1.0. Nevertheless, the model describes forward-delay NMR conditioning as well or better with the default combination of x-shaping parameter values as any other. In particular, the default set yields the best *joint* descriptions of acquisition with various ISIs and response topography. However, the model's performance in this regard depends not only on x-shaping parameters but on other parameters as well: c in Equation 3, β in Equation 7, and the parameters of x, the lag between x and $\dot{x}$ in Equation 8 and δ in Equation 9.

The value of the rate constant c in Equation 3 affects both response topography and

trial-wise learning rate. As shown by Figure 2 of Moore et al (1986), a high value of c, say $c = 0.4$, yields a response topography typical of that observed in well trained rabbits. However, the rate of CR acquisition over trials when $c = 0.4$ is much too fast to be realistic. Values of c low enough to yield appropriate trial-wise increases in weight, e.g., $c = 0.04$, yield an undesirable abrupt transition of response topography from CR to UR at the point of US onset. The value $c = 0.15$ used in the present study represents a compromise between reasonable rates of learning over trials and the realistic response topography. However, it is worth noting that if training consists of one trial per day, robust conditioned NMRs appear within 15 trials (Kehoe and Gormezano, 1974). This rate of conditioning is reasonably in accordance with our simulations of acquisition with $c = 0.15$ and the default values for x-shaping parameters in the model. Kehoe and Gormezano (1974) showed that trial-wise rate of NMR conditioning is directly related to intertrial interval. Unlike some other real-time models (e.g., Moore and Stickney, 1985), the SBD model is not sensitive to this important variable (Moore and Gormezano, 1977).

The value of β in Equation 7 is considered a constant of the SBD model. This parameter determines the rate of decay of the element's output memory, s. Ideally, it should range from 0.5-0.6. If β is greater than 0.6, the ability of the model to reach stable weights is disrupted and a "blow up" in weights occurs. The large weights result in unrealistic rectangular-shaped response profiles. Values of β less than 0.5 result in low amplitude CRs that do not blend with URs and inappropriate negative weights at short ISIs even with a lag between $\bar{x}$ and x in Equation 8 of 30 ms.

The specification of x in Equations 8 and 9 is important for yielding ISIs functions consistent with the literature (Smith et al, 1969). Equation 9 specifies that the rate of the decay of x varies inversely with CS duration. In forward-delay paradigms, this permits V to decline enough during post-US time steps from its on-trial peak to yield an appropriate ISI function when ISI exceeds the optimum of 250 ms. Equation 8, which specifies the time lag between x and $\bar{x}$, is also important for ISI functions. In this and previous reports, $\bar{x}$ lagged x by 40 ms (4 time steps), thereby compensating for large increments of V for CSs of less than 250 ms duration. As noted previously, the lag yields inappropriate negative weights with an ISI of 100 ms (see Moore et al, 1986). We have subsequently discovered that with the default parameter set, a lag of 30 ms (3 time steps) yields small positive rather than negative V with ISIs of 100 ms, and an otherwise appropriate ISI function, provided that β in Equation 7 is 0.5-0.6.

The Input x as a CS Representation and a CR Template

The variable x in the SBD model serves as both a representation of the CS and a template for the CR. As a CS representation, the parameters that govern the rise and decline of x determine such things as rate of increase of V over trials, the shape of learning curves, and ISI functions. As a template, x determines the topography of the CR. This is evident from the fact that with sufficient training CR topography and the shape of x are virtually indistinguishable from each other. Our simulation studies indicate that x can function in both capacities and capture important features of NMR conditioning. Furthermore, it can do so with the same restricted set of parameter values; specifically, those approximately equal to the default set specified in this report.

The current specification of x is not adequate for all aspects of NMR conditioning, however. As noted, no combination of parameter values investigated to date yields an S-shaped learning curve such as those observed in the laboratory. In addition, because x is specified in terms of the onset and offset of the CS, the model cannot yield appropriate CR topographies in either trace conditioning (Moore et al, 1986) or in forward-delay conditioning with a long ISI. As mentioned previously, in the case of long ISIs, for example, CR topographies in the laboratory show inhibition of delay (Pavlov, 1927). That is, CRs begin late in the ISI and increase gradually (ramped rise) so that the maximum amplitude occurs just prior to or concurrent with the US. Hence the CR is *efficient* as well as adaptive. It is adaptive in that the response is timed so that vision is not obstructed unnecessarily before the US. It is efficient in that metabolic energy is not being used to unnecessarily to retract the eyeball during early phases of the ISI. This sort of efficiency is a product of training and is not encompassed by the model. With the default values, x attains 95% of its asymptotic value 300 ms after CS onset, and remains asymptotic until CS termination. However, the results of Schneiderman (1966) indicate that the onset of the conditioned NMR across a wide variety of ISIs occurs roughly halfway through the ISI.

Although our simulation studies indicate that no combination of x-shaping parameters mitigates these limitations of the model, they do suggest approaches to solutions. One approach would be to allow values of parameters m, h, and k to change during training, thereby allowing for production of maximal CR amplitude at the time of the US. Inhibition of delay might be implemented by first using the default x to allow sufficient learning to occur and then implementing an input trace with low values for m and h, like those used in the simulation depicted in Figure 15, to shape the proper topography. Varying the shape of x could also yield S-shaped learning curves. The initial slow rise of the empirically observed learning curve might be achieved by allowing m and h to be low initially. Then, as the number of trials increases, m and h could be increased to their current default

values, thereby allowing the model to describe a negatively accelerated learning curve in later stages of conditioning.

As for trace conditioning, CRs can not occur in the trace interval as long as the rise and fall of x are specified according to the onset and offset of the CS. There are two ways to alleviate this problem. The trivial solution would be to specify that x is defined according to the ISI and not CS duration. However, although such an approach could yield a CR over the trace interval, CR onset might still occur shortly after CS onset, even if the input trace is allowed to change over training as described above. Another way to generate CRs in the trace interval would be to allow CS offset to initiate an input trace to the element at CS offset. This approach is supported by the work of Liu and Moore (1969) which demonstrating that rabbits can be conditioned to respond to stimulus offsets in a forward-delay paradigm. In fact, a model proposed by Desmond and his associates specifies both CS onset and offset processes that are distributed over many input elements (Desmond and Moore, 1987; Desmond et al. 1986).

Problems with the model discussed in this section might be resolved by taking into account interactions between forebrain structures, particularly the hippocampus, and brain stem structures linked to the cerebellum that are important for the conditioned NMR. This possibility will be discussed later.

Neural Implementation of the SBD Model

Several laboratories have demonstrated that the cerebellum plays an essential role in the acquisition and generation of conditioned NMRs (Thompson, Donegan, Clark, Lavond, Lincoln, Madden, Manounas, Mauk, and McCormick, 1987; Yeo et al, 1985a-c; 1986). In this section we discuss two frameworks for implementing the SBD model in cerebellar cortex. We begin by briefly discussing the hypothesis that changes of V occur through modification of parallel fiber (PF)/Purkinje cell (PC) synapses. Although this viewpoint has its detractors (e.g., Llinas, 1985) as well as proponents (e.g., Ito, 1984; Thompson, 1986), there can be no denying the striking similarities between the SB adaptive element as depicted in Figure 1 and the morphology and synaptic organization of cerebellar PCs. Like the SB adaptive element, a cerebellar PC can in principle receive many inputs from parallel fibers arising from many different CSs. The climbing fiber input seems a natural means for providing input from the US, and the cell has basically a single output channel with only limited axon collateralization. Furthermore, cerebellar PCs have been shown to respond to CSs in a CR-related manner (e.g., Berthier and Moore, 1986). We next discuss the possibility that changes of V occur at mossy fiber (MF)/granule cell synapses. This

hypothesis represents a novel approach to cerebellar involvement in classical conditioning, one that may prove to be more consistent with the experimental literature on neural substrates of NMR conditioning than the PF/PC scheme.

Like the SB model, the SBD model also assumes that learning occurs by a modified Hebbian rule: CS weights change proportionally to the extent that the learning element's current output, s, differs from a trace of previous output, $\bar{s}$. These changes occur in the domain of milliseconds. Hence, they are continually altered according to the magnitude and sign of $s - \bar{s}$. If current output is greater than previous output, weights are increased; if current output is less than previous output, weights are decreased. The locus of synaptic modification for a particular CS is presumably some morphologically restricted region wherein synaptic terminals carrying information about the CS can interact with $s - \bar{s}$. In principle, there are a number of ways this interaction might occur.

In the SBD model the relationship between s and $\bar{s}$ is controlled by the parameter β in Equation 7. As noted previously, the model performs best with β in the range 0.5-0.6. Given the 10-ms time step assumed by the model, this narrow range of acceptable β values implies that the relationship between s and $\bar{s}$ can be described in continuous time by an exponential function with a time constant on the order of 30 ms. Hence, for any change in s on a given time step, $\bar{s}$ closes to within one percent of s within the ensuing 10 time steps, or 100 ms. This relationship imposes a constraint on circuit models that would describe where $s - \bar{s}$ is computed and how this term interacts with CS input, x, at sites of synaptic modification.

Any neural circuit capable of implementing the SBD model must specify not only where weight changes occur but also how feedback about NMR topography in the form of the expression $s - \bar{s}$ enters into their computation. Sutton and Barto (1981) suggested that axon collaterals carrying information about $s - \bar{s}$ might feed back onto x input terminals in the form of axoaxonal configurations. The locus of learning in this case would not be within the output neuron but within the terminals or presynaptic entities that carry CS information to the cell. A presynaptic locus of learning would suggest cellular mechanisms such as those invoked in connection with heterosynaptic facilitation of sensitization in *Aplysia* (Hawkins and Kandel, 1984; Walters and Byrne, 1983). However, we know of no evidence for presynaptic mechanisms in cerebellar cortex. Furthermore, Stent (1973) has pointed out that presynaptic implementation of learning is unlikely in vertebrates for reasons we need not pursue here, and he therefore supported the postsynaptic viewpoint.

Alkon (1984) has suggested that the critical postsynaptic events for learning could occur within the restricted volume of a dendritic process that shares synapses of terminals carrying CS information with an adjacent terminal carrying US information. For example,

31

in one neural network implementation of the SBD model discussed below, that in which learning occurs at PF–PC synapses, Alkon's view could be interpreted such that these two inputs would arise from parallel fibers impinging on adjacent spines in the distal arbors of the dendritic apparatus. In terms of the SBD model Alkon's approach would state that the convergence of CS information and feedback information (in the form of $s - \bar{s}$) on a shared dendritic process constitutes the critical learning event. Recall that in the SBD model the US is important for learning only insofar as it contributes to s and hence to the term $s - \bar{s}$. The weight of the US's contribution to s decreases progressively with training: It is implemented by a heuristic (λ') which takes account of the upper limit of s imposed by physiological constraints on the NMR.

In the adaptive element shown in Figure 1, modifiable synapses that would implement the SBD learning rule must be capable of both increases and decreases in efficacy. That is, they are *bidirectional* in the sense that the same synapse must be capable of mediating both EPSPs and IPSPs depending on circumstances of training. For example, the phenomenon of conditioned inhibition (discussed more fully in a subsequent section) is encompassed in the model by having V take on negative value. In contrast to conditioned inhibition, the phenomenon of extinction comes about through unlearning, i.e., by having V lose previously acquired positive value over the course of presentations of the CS without the US.

There is currently little hard evidence for bidirectionality of synaptic weight changes related to learning. Kelso, Ganong, and Brown (1986) report facilitation of associative long term potentiation (LTP) in Hebb-like synapses in hippocampal slices. This facilitation was induced by pairing synaptic activation with injections of depolarizing current into CA1 pyramidal cells. This observation is consistent with Hebbian increases in synaptic efficacy. They also report the prevention of associative LTP induced by injection of hyperpolarizing current. Although the latter observation seems consistent with Hebbian decreases in synaptic efficacy, it does not constitute the establishment of an inhibitory synaptic relationship in the sense of the SBD model.

Cerebellum

Figures 16 and 17 lay the groundwork for discussing schemes for implementing the SBD model and NMR conditioning in the cerebellum. In Figure 16, the numbers 1-3 along the top and letters A-D along the left-hand edge provide a set of coordinates that will facilitate discussion. Figure 16 omits some of details included in most textbook renderings of the cerebellum. For example, climbing fiber synapses onto PCs are not shown. The figure includes only those features needed later for integrating physiological evidence into a plausible circuit diagram for NMR conditioning under the constraints of the SBD model.

32
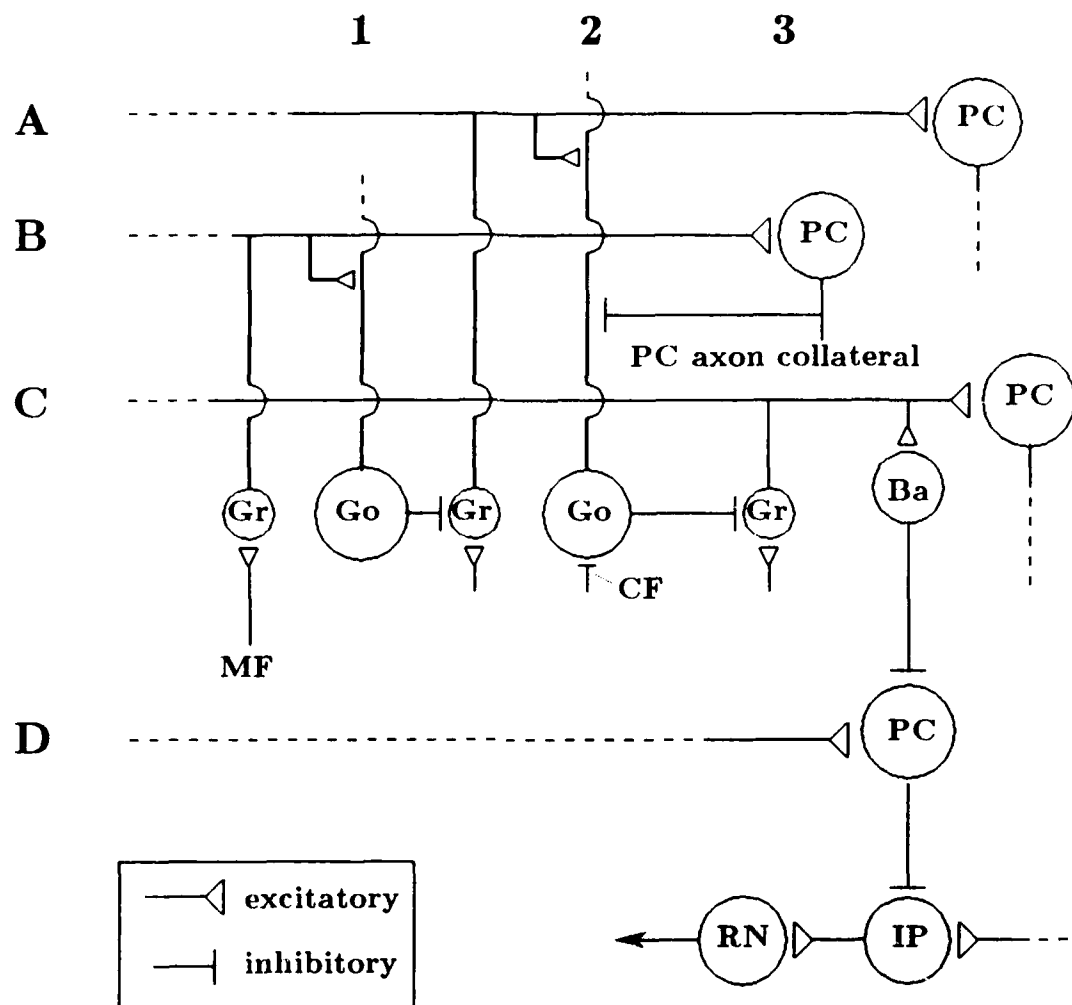
Figure 16. Summary of cerebellar neural circuitry. A-D represent beams of parallel fibers (PF) in the molecular layer. These synapse onto Purkinje cells (PC) and basket cells (Ba), one of which is indicated on the C beam. Basket cells inhibit off-beam PCs, as exemplified by the basket cell on the C beam and the PC on the D beam. The latter is shown as inhibiting a projection neuron in cerebellar nucleus interpositus (IP) which, in turn, excites a projection neuron in contralateral red nucleus (RN) leading to some here-unspecified response. Mossy fiber (MF) terminals and granule cells (Gr) occupy the granular layer. Three granule cells are shown, and two receive inhibitory input from Golgi cells (Go). Both Golgi cells are excited by PF beams. The Golgi cell under 2 is shown receiving two inhibitory inputs, one via a climbing fiber (CF) and another via a PC axon collateral.

33

Figure 17. Summary of cerebellar and brain stem circuitry and information flow mediating NMRs. Solid lines indicate strong projections; dashed lines are used to indicate projections that are comparatively weak or not universally agreed upon. The vertical dashed line represents the medial axis of the brain stem. 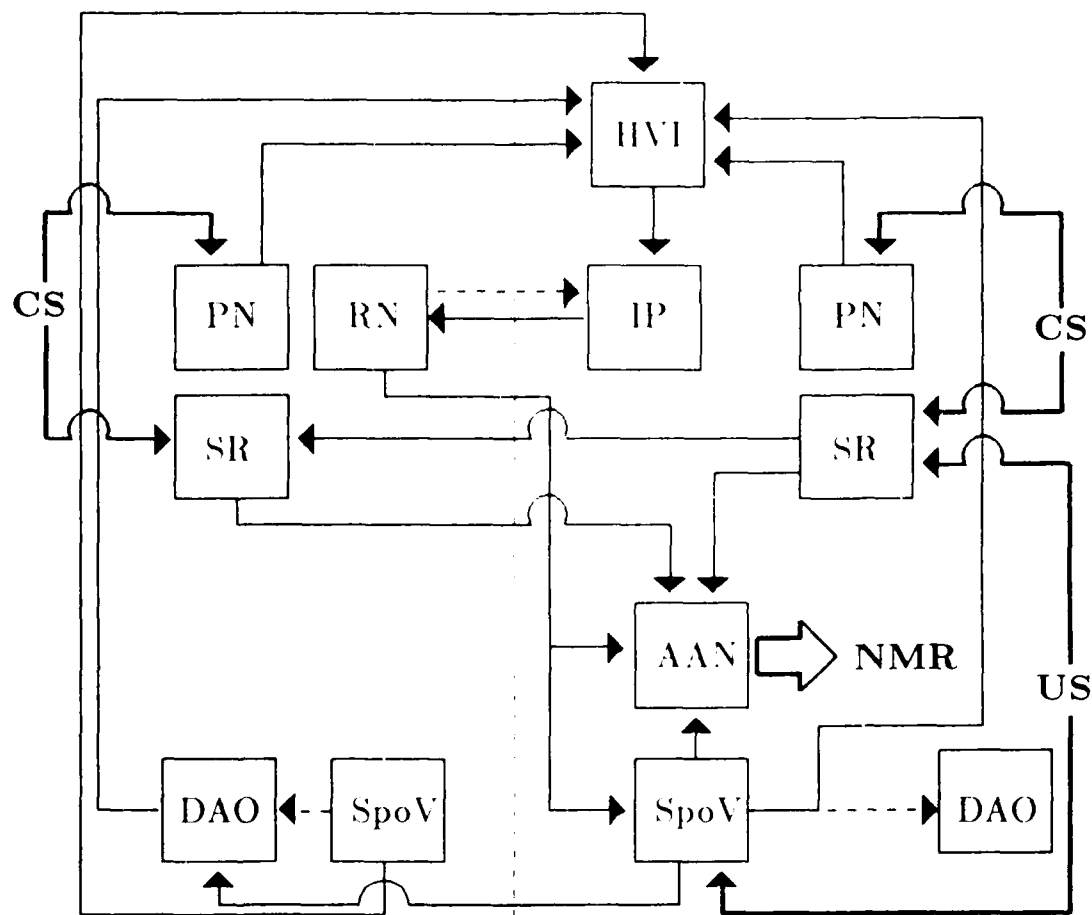CS information (represented bilaterally) gains access to hemispheral lobule VI (HVI) via mossy fibers arising from pontine nuclei (PN). This information, as well as information about the US, also goes to supratrigeminal reticular formation (SR) which is represented bilaterally. SR has been implicated in NMR conditioning as an independent parallel system that appears to be essential for expression of CRs (see Desmond and Moore, 1982; 1986). US information gains access to both SR and HVI via sensory trigeminal neurons. Spinal trigeminal nucleus pars oralis (SpoV) provides synaptic drive to motoneurons in the accessory abducens nucleus (AAN). SpoV also projects to HVI. There is a direct mossy fiber projection and an indirect climbing fiber projection via the dorsal accessory olivary nucleus (DAO). Both sets of projections are bilateral. The output of HVI is relayed to cerebellar nucleus interpositus (IP) and from there to contralateral red nucleus (RN). RN projection neurons terminate in AAN and SpoV to complete the circuit and initiate a conditioned NMR.

Figure 17 summarizes cerebellar and brain stem structures and pathways involved in NMR conditioning (see, e.g., Berthier, Desmond, and Moore, 1987; Thompson, 1986). As noted above, it has been suggested that learning and generation of conditioned NMRs involves cerebellar PCs located in hemispheral lobule VI (HVI). HVI receives acoustic, visual, and somesthetic inputs via the pontine nuclei (see Buchtel, Iosif, Marchesi, Provini, and Strata, 1972; Shofer and Navhi, 1969; Thach, 1967). Lesions of HVI have been reported to dramatically attenuate NMRs (Yeo et al, 1985b), and single-unit recording studies report CR-related patterns of activity by HVI PCs that are consistent with a causal role in this behavior (Berthier and Moore, 1986). Figure 17 shows that the route taken by neural commands initiated in HVI for generation of a conditioned NMR includes several synaptic links. The output of PCs in HVI goes to cerebellar nucleus interpositus (IP); it is then transmitted to contralateral red nucleus (RN). Efferent commands from RN are carried in the rubrobulbar tract as it crosses the midline ventral to the decussation of the brachium conjunctivum. Recent fiber-tracing studies (Robinson, Houk, and Gibson, 1987; Rosenfield, Dovydaitis, and Moore, 1985) suggest that the pathway from RN bifurcates at the level of the seventh nerve. One branch terminates near the accessory abducens nucleus (AAN), where motoneurons chiefly responsible for the NMR are located (Grant and Horcholle-Bossavit, 1986); the other terminates within caudal portions of the principal sensory trigeminal nucleus and spinal trigeminal nucleus pars oralis (SpoV). This second branch from RN participates in the generation of NMRs because SpoV neurons synapse onto AAN motoneurons (Durand, Gogan, Gueritaud, Horcholle-Bossavit, and Tyc-Dumont, 1983). In addition to relaying efferent commands to motoneurons, these neurons could convey feedback about the incipient NMR back to cerebellar cortex via mossy fibers (Ikeda, 1979; Yeo et al, 1985c).

The circuit models discussed below argue for the possibility that the output of cerebellar PCs, s in the model, is fed back to cerebellar cortex for implementation of the learning rule. Based on the information flow described in Figure 16, a likely source for this feedback is brain stem nucleus SpoV. This hypothesis raises questions of timing. Specifically, does CR-related PC activity that initiates the conditioned NMR occur with a sufficiently long lead time so that feedback from SpoV is not obscured by other events such as the occurrence of the US? Berthier and Moore (1986) observed CR-related firing patterns by PCs in HVI that preceded CRs by as much as 200 ms. This is ample time in which to initiate a CR (Moore and Desmond, 1982). Figures 16 and 17 show that there are at least five synapses between PC output and any feedback carried by parallel fibers, and the total conduction distance in the loop could exceed 50 mm. Even allowing 1 ms for each synaptic relay and a relatively slow conduction velocity for myelinated fibers of 20 m/s, circuit time for feedback would require no more than 10 ms, or one time step in the model. As a cautionary note, the conjecture that PCs receive feedback about their output assumes that this information

is transmitted with high fidelity through each link of the chain. That is, the output of neurons in IP, RN, AAN, and SpoV involved in the NMR must match or mirror the output of the PCs. Although evidence is sparse, recording studies indicate that this is probably the case (e.g., Thompson et al, 1987).

Site of Plasticity: Purkinje Cells

Assuming that changes in V in the SBD model occur at PF/PC synapses, where is $s - \bar{s}$ computed and how does this information reach an involved PC? One option is that $s - \bar{s}$ is computed within the PC itself and is therefore readily available to modify eligible synapses. Another possibility that $s - \bar{s}$ is computed outside the PC and fed back by other circuit elements. This could occur in a number of ways (Figure 18). For example, the PC might send an axon collateral to local circuit elements that provide information for computing $s - \bar{s}$. PC axon collaterals have been reported as terminating on Golgi cells, basket cells, granule cells, and other PCs. Were we to rule out feedback from PC axon collaterals, the two remaining sources of feedback are climbing fibers and mossy fibers. For example, feedback information could arise as *efference* from collateral output from SpoV in the course of driving AAN motoneurons: As Figure 17 indicates, in addition to its role as the locus of interneurons mediating unconditioned reflexive extension of the NM to direct stimulation of the eye, SpoV projects to HVI of cerebellar cortex. The projection is either a direct one via mossy fibers, or indirect via climbing fibers originating in the dorsal accessory olive (DAO), the source of climbing fibers to HVI. Both projections could be involved in computing $s - \bar{s}$.

Having designated SpoV as a likely source of feedback used to compute $s - \bar{s}$, consider the various ways this information might reach a PC for modification of PF/PC synapses. These are summarized in Figure 18. Figure 18A indicates several alternative means by which $s - \bar{s}$ might attain access to the PC, including the possibility noted above that it is computed within the cell. The extracellular routes include parallel fibers (PF), the climbing fiber (CF), or an indirect route via a basket cell (Ba). Yet another set of possibilities, shown in Figure 18B, is that one of the variables, either s or $-\bar{s}$, is generated within the PC and the other term is contributed extracellularly. All of the schemes illustrated in Figure 18 require that computation of $s - \bar{s}$ does not compromise the PC's assumed role in generating CRs.

Site of Plasticity: Granule Cells

Because of doubts expressed by a number of investigators about learning mediated by modification of PF/PC synapses (e.g., Bloedel and Ebner, 1985; Lisberger, Morris, and Tychsen, 1987; Llinas, 1985), we considered the possibility that learning occurs at

MF/granule cell synapses. We propose that granule cells compute changes in V via convergence of $s - \bar{s}$ from Golgi cells and x conveyed by mossy fibers. This convergence of $s - \bar{s}$ and x implements the bidirectional Hebbian mechanism assumed by the model.

Golgi cells appear to be particularly suitable for computing $s - \bar{s}$ for several reasons:

1. They receive input from a variety of sources, the principal ones being parallel fibers and mossy fibers. They also receive collateral inputs from PCs and climbing fibers. Hence, in principle they could provide sites of convergence of information about s and $\bar{s}$ for computation of $s - \bar{s}$.

2. The output of Golgi cells varies smoothly as a function of input. Their tonic rate of discharge is regular with little moment-to-moment fluctuation in interspike intervals that could degrade information flow through the granular layer. Hence, they are capable of modulating their output to reflect their input with little noise or signal distortion (Miles, Fuller, Braitman, and Dow, 1980; Schulman and Bloom, 1981). This is a desirable feature of any circuit element that would transfer feedback about NMR topography with high fidelity.

3. In addition to Golgi cell/granule cell interactions within the granular layer, rabbits possess an extra, mid-molecular sheet of "ectopic" Golgi cells and associated glomeruli that may coordinate interactions among mossy fibers and granule cells (Spacek, Parizek, and Lieberman, 1973). The synaptic organization among elements in this mid-molecular sheet appears to be no different from that of the granular layer. Though purely speculative, this extra sheet of Golgi cells may enhance information processing related to learning.

4. According to a study by Eccles, Sasaki, and Strata (1967), the temporal course of Golgi cell inhibition of information flow through the granular layer resembles the relationship between $\bar{s}$ and s in the SBD model. We suggest that Golgi cells compute $\bar{s}$ by acting on granule cells that receive s information simultaneously from mossy fibers. Possible circuits by which s and $\bar{s}$ converge onto other Golgi cells for computation of $s - \bar{s}$ will be considered later. First, a digression describing the Eccles et al (1967) experiment is indicated.

Using anesthetized cats as subjects, Eccles et al (1967) analyzed field potentials in cerebellar cortex (vermis and lobus simplex, which in cat corresponds to HVI in rabbit) evoked by stimulation of mossy fibers. Stimulation of parallel fibers inhibited the response evoked by mossy fiber stimulation. This inhibition was mediated either by Golgi cells or by basket cells. Golgi cell inhibition could be discriminated from basket cell inhibition by a number of criteria. Golgi cell inhibition required on-beam stimulation, reached a maximum

A
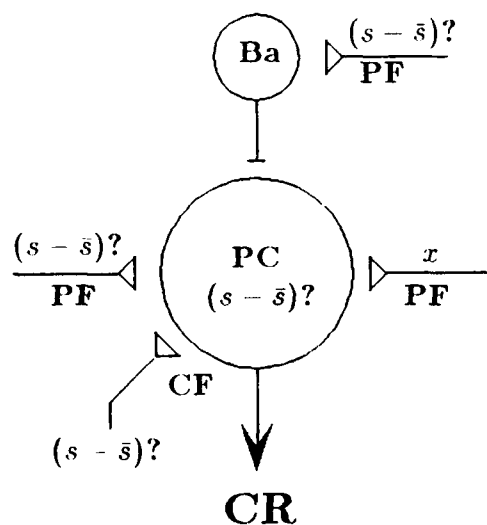
B
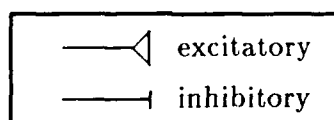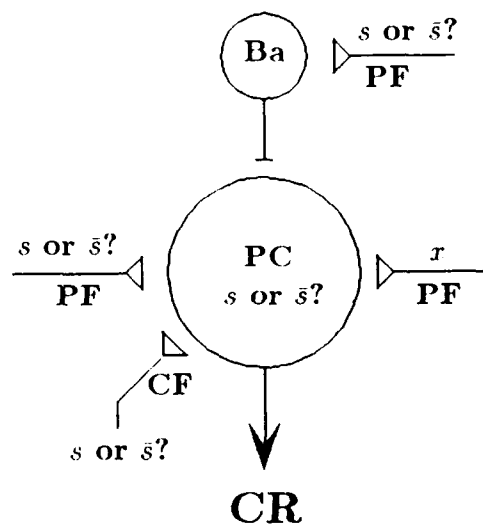
Figure 18. Summary of possible sites of convergence of SBD model variables x and $s - \bar{s}$ for weight changes mediated by parallel fiber/PC interactions. Diagrams A and B represent PCs with two parallel fiber (PF) inputs, a climbing fiber (CF) input, and a basket cell (Ba) input. In Figure 18A $s - \bar{s}$ might be transmitted to the PC by any route or it might be computed intracellularly. In Figure 18B the two components of $s - \bar{s}$ are dissociated from each other so as to illustrate the possibility that each is contributed from a different source.

within 10 ms, and decayed exponentially with a time constant of approximately 30 ms so that inhibition was essentially complete after 100 ms. By contrast, basket cell inhibition could be evoked by off-beam stimulation, peaked within 35 ms, and persisted for up to 400 ms. Although Golgi cell inhibition in the protocol used by Eccles et al may hold only when background activity is low, e.g., as in the case of an anesthetized preparation (Bloedel and Roberts, 1969), its temporal course nevertheless coincides with the relationship between s and $\bar{s}$ in the SBD model in the temporal domain with $\beta = 0.5$-0.6. This coincidence of the time course of Golgi cell inhibition and the temporal relationship between s and $\bar{s}$ in the SBD model suggests that Golgi cells participate in computation of $\bar{s}$. These Golgi cells, and the granule cells they impinge upon, are different from the ones indicated at the beginning of this section that compute $s - \bar{s}$ and implement the learning rule at MF/granule cell synapses.

Figure 19 summarizes how Golgi cells compute $\bar{s}$ in the way suggested by the Eccles et al (1967) study: s information carried by mossy fibers is converted to $\bar{s}$ by the action of Golgi cells. The model assumes that Golgi cells that convert s to $\bar{s}$ are activated by parallel fibers. A group of granule cells (Gr), represented in the lower left hand portion of the figure, receives mossy fiber input carrying s information as feedback from SpoV (coordinate C1). The output of these granule cells passes s information through the granular layer with no distortion to form parallel fiber beam B. Beam B excites Golgi cells (Go) that impinge on members of a second class of granule cells that also receive s via mossy fibers from SpoV. We emphasize that these Golgi cells and the second class of granule cells receive s simultaneously, i.e., within the same 10 ms time step. The action of the Golgi cells on the second group of granule cells converts s to $\bar{s}$. The output of the second group of granule cells forms the parallel fiber beam labeled A which transmits $\bar{s}$ to other circuit elements.

There is some evidence for the existence of two classes of granule cells with response characteristics similar to those envisioned by our circuit model. Recording from presumed granule cells (granular layer input elements or GLIES) in monkey flocculus during saccadic eye movements, Miles et al (1980) observed units that burst during a saccade and other units that respond with a slower rate of firing which decays with time constants in the range 10-50 ms (see Miles et al, 1980, Fig. 2, p 1446). The former are analogous to the first class of granule cells in the model, in which s passes through the granular layer without modulation; the latter are analogous to the second class of granule cells in the model, in which s is converted to $\bar{s}$ by Golgi cell inhibition.

The circuit model assumes that learning occurs at synapses of granule cells that receive mossy fiber input labeled r (coordinate C3). Mechanisms that implement the eligibility of these synapses for modification, r, presumably reside within these granule cells. The

Figure 19. Implementation of SBD model at mossy fiber/granule cell synapses. A-C are parallel fiber beams as in Figure 17. From right to left: the variable s is fed back to cerebellar cortex by mossy fibers arising in brain stem spinal trigeminal nucleus pars oralis (SpoV in Figure 17) in two streams. One stream gives rise to parallel fibers that drive PCs with a firing pattern that lags the CR. This beam (B) excites Golgi cells (Go) that impinge on granule cells (Gr) excited by the other stream carrying s and thereby convert it into a beam of parallel fibers (A) carrying $\bar{s}$ information. This beam drives PCs with a firing pattern that lags the CR and is damped relative to the firing patterns of PCs on beams B and C. Beam A contributes $\bar{s}$ to Golgi cells that compute $s - \bar{s}$. The other term for this computation, s, is provided either by axon collaterals from lag PCs on the B beam or by climbing fibers. These Golgi cells pass $s - \bar{s}$ to granule cells that receive CS information, x, and thereby mediate weight changes at these mossy fiber/granule cell synapses to the extent that they are eligible for modification. These granule cells give rise to a beam of PFs (C) that drive PCs proportionally to Vx and with a firing pattern that leads the CR.

factor $s - \bar{s}$ is contributed by Golgi cells that function as differential amplifiers. These Golgi cells receive s as excitatory input from Beam A (coordinate A2), as described above. In Figure 19, they receive $\bar{s}$ as an inhibitory input (direct or indirect) from climbing fibers (coordinate C2). Later on, we suggest that this climbing fiber input for the variable $\bar{s}$ might be replaced by input from a PC axon collateral such as the one indicated at coordinate B3. The climbing fiber input is omitted in a subsequent, more complete version of the model described later on. Notice that the Golgi cell under 2 in the figure is actually computing $\bar{s} - s$. We have referred to the computation as being $s - \bar{s}$ in interests of clarity. Because Golgi cells are inhibitory, the computation is *effectively* one of $s - \bar{s}$ with respect to the granule cells receiving r.

Because Golgi cells are inhibitory interneurons, when $s - \bar{s}$ is positive the tonic output of the Golgi cells is modulated downward, thereby disinhibiting granule cells that receive r on which they impinge. This disinhibition causes an increase in the weight of MF/granule cell synapses to the extent that they are eligible for change. Similarly, when $s - \bar{s}$ is negative the tonic output of these Golgi cells is modulated upward. This increases granule cell inhibition and decreases the weight of eligible MF/granule cell synapses. The feasibility of bidirectionality of weight changes is suggested by the work of Kelso et al (1986), mentioned above, and theoretical analyses of calcium dynamics in dendritic spines by Gamble and Koch (1987).

In order to provide a continuum of possible values of $s - \bar{s}$, Golgi cells must be able to vary their output over a reasonably wide range of firing frequencies. Schulman and Bloom (1981) report average Golgi cell firing rates of about 20 Hz in rat and Guinea pigs. This rate is roughly comparable to that of presumed Golgi cells observed in monkey flocculus by Miles et al (1980). Miles et al noted a wide range of firing rates (10-80 Hz) and smooth variation between these frequencies during pursuit eye movement.

Finally, the circuit model specifies two active roles for Golgi cells: One is computation of $\bar{s}$ as outlined above, and the other is computation of $s - \bar{s}$. Palay and Chan-Palay (1974) note that the distribution of Golgi cell circumferences is bimodal, with the first peak occurring in the range of 9 to 16 μms ("large" Golgi cells) and the second in the range of 6 to 11 μms ("small" Golgi cells). The existence of two categories of Golgi cells may imply a difference in the types of computation each performs.

CR-Related PC Activity: Lead, Lag, and Damped Lag

The circuit model in Figure 19 (and subsequently Figure 20) implies the existence of various types of CR-related firing patterns by PCs. For example, the PC on the s beam (A) is labeled "damped lag" because its firing pattern during a CS presentation

would lag behind a CR and would also reflect the slow rise and decay of spike recruitment implied by the relationship between $\dot{s}$ and s in the model. The PC on the s beam (B) is labeled "lag" because its firing rate during a CS presentation would mirror response topography but with a lag by virtue of the fact that s represents efference from the brain stem. CR-related "lead" PCs such as the one on the x beam (C) are also implied by the circuit. Berthier and Moore (1986) observed both lead and lag CR-related PCs in HVI during NMR conditioning. They also observed PCs that decreased their firing before the occurrence of CRs. These CR-related "off-cells" of the lead type will be discussed below.

The existence of both lead and lag cells suggest that cerebellar cortex might be doing more than simply computing weight changes that give rise to CRs. Many elements in the circuit model shown in Figures 19 and 20 have been invoked to explain a variety of timing functions, e.g., lead-lag compensation (for an overview see Llinas, 1970; see also Hassul and Daniels, 1977; Marr, 1969). Our considerations about how cerebellar cortex might implement the SBD model for NMR conditioning are not intended as arguments against any of these timing functions.

Role of Climbing Fibers

Some investigators have expressed strong reservations regarding climbing fiber participation in classical conditioning (see, e.g., Llinas, 1985). Particularly contentious has been the idea that climbing fibers carry US information that reinforces learning in cerebellar cortex (e.g., Thompson, 1986). In the circuit implementation of the SBD model shown in Figure 19, climbing fibers contribute to learning only insofar as they might provide feedback about s to Golgi cells that compute $\dot{s} - s$. A way this might be achieved without climbing fibers is also illustrated in Figure 19. Instead of using climbing fibers, s might be transmitted to the Golgi cells by axon collaterals from lag PCs on the parallel fiber beam labeled B (coordinates B3). A circuit based on PC collaterals circumvents the computational difficulties implied by the low frequency of climbing fiber firing while at the same time retaining the desirable inhibitory effect on the Golgi cells. Figure 19 shows these collaterals arising from lag PCs instead of lead PCs on beam C which might serve as well from a computational standpoint. This is because PC collaterals are not generally oriented along the longitudinal axis of a parallel fiber beam, as would be the case if they arose from PCs on the C beam. Instead, PC collaterals are oriented perpendicularly to the longitudinal axis (Ito, 1984), as would be the case if they came from PCs on an adjacent beam of parallel fibers such as B.

The idea that climbing fibers might convey s to Golgi cells was suggested by the Schulman and Bloom (1981) report of Golgi cell inhibition in response to stimulation of climbing fibers and by morphological evidence that climbing fibers contribute to mossy fiber
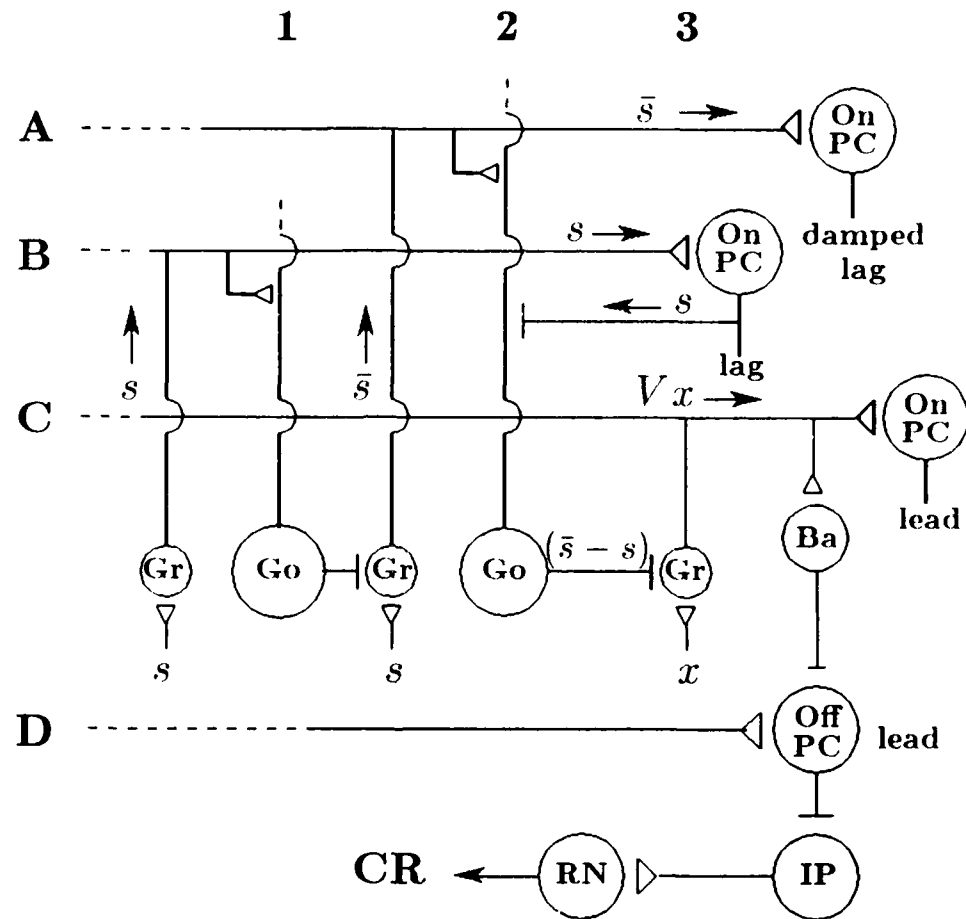
42

Figure 20. Summary of cerebellar neural circuitry summarizing how basket cells (Ba) added to the parallel fiber beam (C) of Figure 19 can account for off-type lead CRs observed by Berthier and Moore (1986). CS onset excites beam C parallel fibers and thereby driving basket cells that inhibit tonic firing of PCs on the D beam. These off PCs of the lead type disinhibit IP neurons and thereby initiate the sequence of motor commands that result in a CR.

en Marron synapses onto Golgi cells (Ito, 1984). Schulman and Bloom suggested that the inhibition they observed was likely not direct but mediated by basket cells. However, to our knowledge direct basket cell projections to Golgi cells have not been reported in the anatomical literature.

Another difficulty with climbing fibers is that their firing rates may be too low (tonically 1-2 Hz) to faithfully carry information about s with a temporal resolution adequate for computation of $s\text{—}s$ in the millisecond domain. Although Berthier and Moore (1986) observed a few instances of climbing fiber volleys (complex spikes) related to CRs, these climbing fiber volleys consistently led CRs, thus making it unlikely that they were carrying feedback information. The highest observed momentary rate of CR-related complex spiking was on the order of 10 Hz. By contrast, our implementation of neuronal firing by the SBD element assumes firing rates up to 200 Hz, and rates of simple spike firing in cerebellar PCs as high as 400 Hz have been reported. The low frequency of CR-related climbing fiber activity may not preclude an alternative computational model incorporating climbing fibers.

What role if any might we assign to climbing fibers if they do not contribute to computation of $s\text{—}s$? Experimental evidence on the contribution of climbing fibers in NMR conditioning is controversial and open to interpretation. Thompson (1986) cites evidence that stimulation of DAO, the source of climbing fibers to HVI, reinforces conditioning. Consistent with this idea, he also reports that lesions of this structure cause a gradual extinction of the CR following training with an air puff US. The stimulation results might reflect unintended antidromic activation of SpoV neurons and concommitant invasion of collaterals of mossy fibers that project to HVI (see Figure 17). As for the lesion data, Yeo et al (1986) report that DAO lesions cause an immediate disruption of NMR conditioning, not a gradual loss of CRs that would be expected if climbing fibers carry information that reinforces conditioning. A sudden and persistent loss of CRs such as that reported by Yeo et al (1986) would be expected if climbing fibers perform some trophic function such as regulating PC excitability, as has been suggested by numerous investigators (e.g., Bloedel and Ebner, 1985; Strata, 1985).

Berthier and Moore (1986) found little support for the idea that climbing fibers carry US information related to reinforcing learning. They observed only a few cases of complex spikes elicited by the US employed in their study. However, these data were obtained after sufficient training to ensure that CRs occurred on a high proportion of trials. The likelihood of observing climbing fiber responses to the US might be greater during earlier stages of CR acquisition, i.e., when $s\text{—}s$ at US onset would be consistently large.

44

CR-Related PC Activity: On and Off

As noted, Berthier and Moore (1986) observed PCs that increased their simple spike firing above pre-trial rates on trials with CRs. These cells were designated "on cells". However, CR-related "off-cells", PCs that decreased their firing rate below pre-trial rates, were also observed. Although off-PCs might arise from long term depression of PF/PC synapses (Ito, 1984; Thompson, 1986), the circuit model shown in Figure 20 provides an alternative explanation of off-PCs. These PCs are associated with the beam of parallel fibers labeled D. They become off-cells of the lead type when a CS is presented because of increased inhibition from basket cells (Ba) on the C beam (coordinate D3). (Like PC axon collaterals, basket cell axons tend to project perpendicularly to the longitudinal axis of the parallel fiber beam by which they are activated).

A CR is initiated when basket cell inhibition of PCs on beam D becomes sufficiently great to *disinhibit* IP neurons to which they project. These IP cells project in turn to RN neurons that excite the reflex pathways mediating the CR (Figure 17). Because mossy fibers from pontine nuclei do not send collaterals to deep cerebellar nuclei (Brodal, Dietrichs, and Walberg, 1986), the model does not assume that CSs activate IP neurons. They are assumed to be tonically activated by neural traffic unrelated to a particular stimulus, but this activation is normally suppressed by inhibition imposed by PCs. Hence, a CS releases this inhibition and the level of activation of IP neurons increases sufficiently to drive the RN neurons in the next stage of the efferent pathway of the CR.

In order for CRs to be generated by on-PCs instead of off-PCs, there would have to be a signal inversion somewhere downstream in the efferent circuit, e.g., at the level of RN (see Figure 17). On-PCs would inhibit IP neurons that project to RN, and this would lead to off-type CR-related responses by RN units. Although CR-related on-units in RN are commonly observed during NMR conditioning, off-units are rare (J.E. Desmond, personal communication).

Since off-PCs are attractive candidates for generating CRs, is it possible that they arise through some other means? Besides the possibility of long term depression noted above, one way to generate CRs without the posited intermediary basket cell would be to invert the variable x before it is transmitted to cerebellar cortex. Such an inversion would manifest itself as an inhibitory action of mossy fibers carrying CS information on granule cells. However, CSs such as acoustic stimuli are known to excite cells in the granular layer (Snider and Stowell, 1944), and therefore signal inversion on the input side is an untenable means of evoking off-type responses in PCs.

In order to mediate the generation of CRs, basket cells on the C beam must begin to

inhibit PC's on the D beam sufficiently soon after CS onset to ensure CR initiation within the temporal window defined by the CS-US interval. As noted above, Eccles et al (1967) found that basket cell inhibition evoked by off-beam parallel fiber stimulation peaks with a latency of 35 ms and persists for up to a few hundred ms. These characteristics of basket cell inhibition might explain why behavioral CRs rarely have latencies less than 100 ms and are seldom sustained for more than a few hundred ms. It seems plausible that basket cells participate in the adaptive shaping of CR topography thought to underly inhibition of delay, i.e., the acquired tendency for peak CR amplitude to occur just before the expected time of occurrence of the US.

Assuming off-PCs mediate CRs, how are we to interpret on-PCs that lead the behavior? Clearly their existence implies inhibition of deep nuclear cells in IP to which they project, and such off-units have been observed in our laboratory in recording from IP during NMR conditioning. It is likely that on-PCs that lead CRs reflect parallel learning associated with processes such as stimulus coding, response shaping, or concommitant behaviors normally inhibited during a CR.

Figure 21 summarizes the four types of firing patterns discussed in connection with Figure 20. As in the Berthier and Moore (1986) study, the interval between CS onset and US onset represents 350 ms. The CR in the figure begins 200 ms after the CS. Renderings of PC simple-spike firing were hand-crafted to resemble typical CR-related PC responses; they all assume baseline firing rates of 100 Hz, which is typical of that observed in our recording experiments. The firing patterns are labeled to correspond with the types of PCs indicated in the circuit model shown in Figure 20. Hence, the increase in firing rate of the Lag On-PC begins within a few ms after CR initiation. The increase in firing of the Damped Lag On-PC begins slightly later and persists slightly longer. The increase in firing rate of the Lead On-PC precedes the CR by more than 100 ms, and the Lead Off-PC begins to cease firing at this time, both profiles being typical of CR-elicited firing patterns observed by Berthier and Moore (1986).

Of the approximately 40 CR-related PCs reported by Berthier and Moore (1986), on-cells exceeded off-cells by 3:1, and lead and lag cells were equally distributed (ratio of 1:1). Although possibly a coincidence, it is nevertheless interesting that these ratios are implied by the circuit model, provided of course that parallel fiber beams A-C are comparable in terms of number of fibers and levels of activation evoked by the variables $\bar{s}$, s, and r, respectively. The correspondence between the model's predictions regarding the statistical distribution of CR-related PC types encourages further experimental tests of the model. Such experiments might provide: (a) reliable separation of damped-lag PCs from the lag PCs; (b) evidence of Golgi cell activity related to the variables s or $\bar{s}$, i.e., the implied but

46

Lead On-PC

Lead Off-PC

Lag On-PC

Damped
Lag On-PC
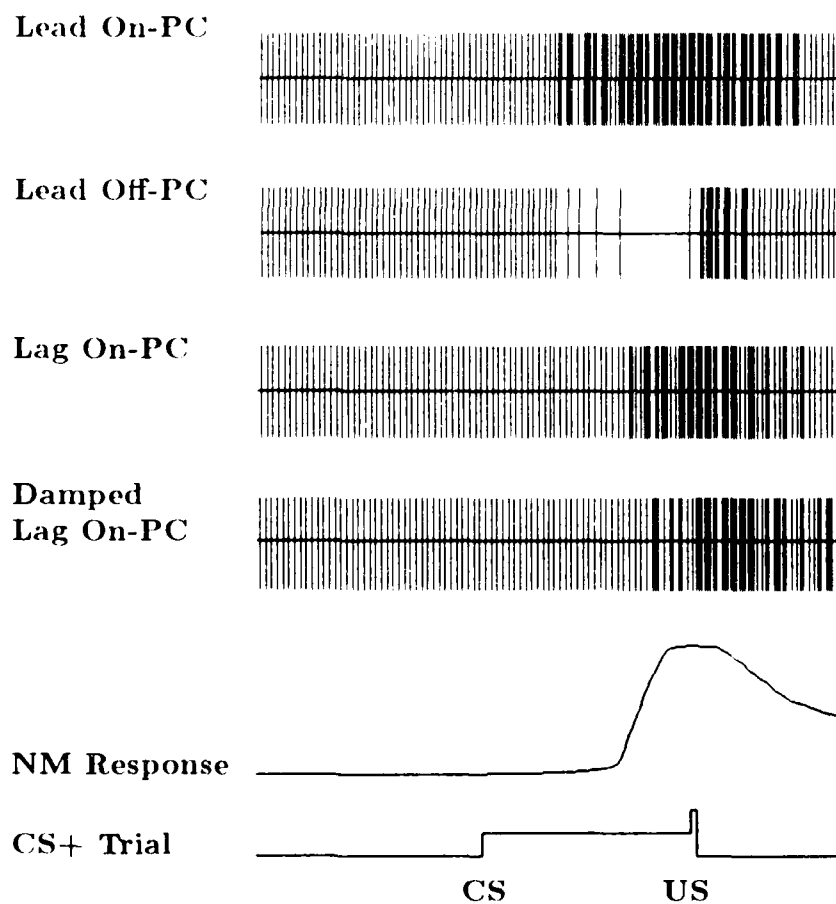
NM Response

CS+ Trial

CS   US

Figure 21. Renderings of CR-related simple spike firing patterns predicted by the circuit model in Figure 20. The baseline firing frequency for all four types of PCs is 100 Hz, and the CS-US interval on reinforced trials (CS+) is 350 ms.

as-yet-unsubstantiated CR-related firing of the lag and damped-lag variety among Golgi cells; (c) evidence of CR-related neural traffic among parallel fibers (beams A-D in Figure 20).

Cerebellar Implementation of Multiple-CS Phenomena

In this section we discuss the implications of a cerebellar circuit implementation of the SBD model for multiple-CS phenomena. Our effort to implement the SBD model in cerebellar cortex was guided by experimental evidence suggesting that this region of the brain is not only essential for robust CRs, but may be a site of learning as well. We have argued that a circuit implementation along the lines of Figure 20 is a promising candidate for implementing the model, but our discussion has been limited to conditioning with a single CS. How adequate is this implementation for conditioning protocols involving more than one CS? If the implementation is problematic from the viewpoint of relevant data the difficulty might lie with the model, with the circuit, or with its assigned locus within the brain.

The principal multiple-CS phenomena of interest are higher-order conditioning, blocking, and conditioned inhibition. Like virtually all contemporary learning theories, including the original SB model (Barto and Sutton, 1982), the SBD model predicts appropriate outcomes in simulations of these multiple-CS protocols (Blazis et al, 1986; Moore et al, 1986). The model predicts higher-order conditioning because it is basically an S-R contiguity theory of learning, albeit one with an informational structure: A second-order CR can be established provided the temporal relationship between the primary and secondary CSs is appropriate and provided the primary, initially trained CS is capable of evoking a CR. Should the primary CS lose its capacity to evoke a CR, e.g., through extinction, the secondary CS would eventually follow suit. The model predicts blocking because of its perceptron-like architecture as depicted in Figure 1 and the fact that the learning rule in Equation 3 is basically a variant of the Widrow-Hoff rule (see Sutton and Barto, 1981). Conditioned inhibition also follows from Equation 3 because the synaptic weight, V, of a CS that is never reinforced can take on negative value when it is presented in combination with another CS that possesses a consistently positive weight. Hence, conditioned inhibition depends on the bidirectionality of the Hebbian mechanism for synaptic modification discussed previously.

The circuit model in Figures 19 and 20 could readily be extended to encompass higher-order conditioning and blocking. All that would be required is a global broadcast of the variables s and $\bar{s}$ over a sufficiently large region of HVI to encompass inputs from many potential CSs. This would permit local computation of $s - \bar{s}$ by Golgi cells. In the case of higher-order conditioning, synaptic weights at granule cells that receive input from the

48

second-order CS would increase to the extent that they remain eligible for change at the time their associated Golgi cells compute the large negative value of $\dot{s}$—s that results from evocation of a CR by the primary CS. Should the primary CS lose weight, the weight of the secondary CS would decline as well. In blocking, the CS combined with the originally trained CS would not accumulate weight gains over reinforced trials as long as the original CS retained the capacity to evoke a CR; a CR sufficiently robust to preclude large values of s—$\dot{s}$ at the time of US onset. However, extending the circuit model in the manner suggested here would not be appropriate because of experimental evidence indicating that blocking, higher-order conditioning, and certain other complex conditioning phenomena involve the participation of other brain regions besides the cerebellum, particularly the hippocampal formation.

The idea of global broadcasting of s and $\dot{s}$ would also allow for the creation of negative weights in granule cells that receive input from a CS assigned the role of conditioned inhibitor. However, in addition to being resistant to subsequent acquisition procedures, a conditioned inhibitor must be capable of opposing the evocation of a CR by a conditioned exciter when the two stimuli are presented together. It is not obvious how this would be accomplished in the cerebellar circuit model. It may be inappropriate to alter the present circuit model so as to produce such CR suppression, in any case, because there is no evidence that the cerebellum is involved in conditioned inhibition of the NMR. For example, Berthier and Moore (1986) used a differential conditioning procedure in order to assess the CR-relatedness of cerebellar units. Differential conditioning is closely related to conditioned inhibition in that both procedures include reinforced and nonreinforced trials. Although CRs were suppressed on a high proportion of trials to the nonreinforced CS, there were no instances of unit activity related to CR suppression. Furthermore, lesion studies by Mis (1977) and others suggest that conditioned inhibition involves the participation of brain regions outside the cerebellum (see Yeo, Hardiman, Moore, and Steele-Russell, 1983). If conditioned inhibition involves processes extrinsic to the cerebellum, as seems likely, there may be no need to assume a bidirectional Hebbian mechanism in the model. Learning theorists have long recognized that bidirectional modifiability is not necessary to account for conditioned inhibition (e.g., Moore and Stickney, 1985).

In sum, the SBD model is a mathematical description of a device capable of simulating an impressive array of facts about NMR conditioning at the behavioral and neurophysiological levels. Despite its potential ability to encompass multiple-CS effects within the framework of either a single neuron resembling Figure 1 (e.g., Figure 18) or a somewhat more elaborate circuit (e.g., Figures 19 and 20), an implementation of the model confined to the cerebellum is not entirely appropriate for multiple-CS phenomena. This caveat aside, our investigations of the SBD model have nevertheless suggested a novel theory

49

about the locus of synaptic changes for a real instance of conditioning and in a real nervous system. Further theoretical work should move toward a systems level of analysis that might point the way toward to a neural network architecture that not only accounts for phenomenology, but does so in a neurobiologically realistic manner. Further research on the circuit model could be conducted on a time scale compatible with the modeling of neural events such as action potentials, that is, in the domain of microseconds.

Neurobiological Correlates of x: Pons and Hippocampus

Implementing the SBD model in the cerebellar cortex raises questions as to how CS input is shaped so as to yield appropriate response topography, that is, what are the mechanisms that provide the preprocessing of CS inputs to learning elements? In this section we discuss the possibility suggested by several investigators that such preprocessing involves interactions among the cerebellum, hippocampus, and pontine nuclei (see Berger, Weikart, Bassett, and Orr, 1986; Schmajuk, 1986). Basically, the idea is that CR templates are constructed in parallel and at multiple levels. At the level of pontine nuclei, stimuli are coded with respect to onsets and offsets. Although this would suffice for adaptive CR topographies in forward-delay paradigms with near-optimal ISIs, more elaborate coding schemes involving the hippocampus and cerebellum are engaged in more complex paradigms such as trace and long-ISI paradigms.

Berger et al (1986) have described a circuit involving hippocampus, subiculum, retrosplenial cortex, and pontine nuclei that could provide for hippocampal modulation of CS information conveyed over mossy fibers to putative learning elements in cerebellar cortex. Port, Mikhail, and Patterson (1985) cite evidence supporting the notion that the hippocampus provides a neural template of the CR that develops over training. Its influence on response topography depends on the complexity of the paradigm. Without the neural template, response timing and amplitude are compromised in paradigms with nonoptimal ISIs. Solomon, Vander Schaaf, Norbe, Weisz, and Thompson (1986) reported that hippocampectomized rabbits display short-latency CRs during trace conditioning, relative to sham-operated controls; these CRs bear a striking resemblance to those predicted by the SBD model under trace conditioning protocols. However, other workers have found longer-than-normal CR latency during trace conditioning of hippocampectomized rabbits (Port, Romano, Steinmetz, Mikhail, and Patterson, 1986).

Recording studies provide further evidence for hippocampal involvement in the shaping of response topography. Conditioning-related neuronal activity occurs in the hippocampus during forward-delay training and such activity models the behaviorally observed response

50

(Berger, Laham, and Thompson, 1980). Hoehler and Thompson (1980) recorded behavioral CRs and hippocampal unit activity in rabbits that were first trained to respond to a 250 ms CS and which were then presented with 500 ms CSs. Both the behavioral CR and the hippocampal unit response were shown to peak near the time of US onset, with the hippocampal peak occurring 30 to 60 ms prior to the peak of the behavioral CR. However, when the rabbits were switched to presentations of a 500 ms CS, both the hippocampal activity and the behavioral CR shifted, but the shift in the hippocampal response occurred sooner.

We have suggested that the preprocessor needed by the SBD model should be capable of altering parameters that shape x, thereby providing the necessary modulation of the amplitude and time course of a response. We have noted that the proper combination of m and h can yield longer-latency CRs. However, changing the shape of x is not sufficient for appropriate topography in the trace conditioning paradigm, since x begins to decay at CS offset. The pre-processor (hippocampus) might override this problem by shifting x so that the rising phase of the CR begins after CS offset. Implementing a mechanism for changing the shape of, or shifting x could be based on feedback about the adaptability of the template presumably provided by the hippocampus under conditions of non-optimal ISIs or trace conditioning. There is evidence that the contribution of the hippocampus to NMR conditioning might be partially mediated by feedback via projections from cerebellum, as suggested by loss of CR-related hippocampal neuronal firing following lesions of cerebellum (Clark, McCormick, Lavond, and Thompson, 1984).

The present report has examined our effort to model CR topography by shaping CS input to a learning element in such a way as to provide a template for the response to be learned. The critical questions concern how and where the CS is represented within the brain. At this time, the most promising brain region may be the pontine nuclei, structures which form points of convergence of sensory inputs and possibly response modulating inputs from the hippocampus. Simultaneous recordings from pons and hippocampus, as well as hippocampus and cerebellum, may further elucidate the information processing underlying NMR conditioning.

Acknowledgements

REFERENCES

Alkon, D.L. Calcium-mediated reduction of ionic currents: A biophysical memory trace. *Science*, 226: 1037-1045 (1984).

Barto, A.G. and Sutton, R.S. Simulation of anticipatory responses in classical conditioning by a neuron-like adaptive element. *Behavioural Brain Research*, 4: 221-235 (1982).

Berger, T.W., Laham, R.I., and Thompson, R.F. Hippocampal unit-behavior correlations during classical conditioning. *Brain Research*, 193: 229-248 (1980).

Berger, T.W., Weikart, C.L., Bassett, J.L., and Orr, W.B. Lesions of the retrosplenial cortex produce deficits in reversal learning of the rabbit nictitating membrane response: implications for potential interactions between hippocampal and cerebellar brain systems. *Behavioral Neuroscience*, 100: 802-809 (1986).

Berthier, N.E. The role of the extraocular muscles in the rabbit nictitating membrane response: a reexamination. *Behavioural Brain Research*, 14: 81-84 (1984).

Berthier, N.E. and Moore, J.W. Role of extraocular muscles in the rabbit *(Oryctolaus cuniculus)* nictitating membrane response. *Physiology & Behavior*, 24: 931-937 (1980).

Berthier, N.E. and Moore, J.W. Cerebellar Purkinje cell activity related to the classically conditioned nictitating membrane response. *Experimental Brain Research*, 63: 341-350 (1986).

Berthier, N.E., Desmond, J.E., and Moore, J.W. Brain stem control of the nictitating membrane response. In I. Gormezano, W.F. Prokasy, and R.F. Thompson (Eds.), *Classical conditioning, 3rd edition*. Hillsdale, N.J.: Lawrence Erlbaum Associates, 1987, 275-286.

Blazis, D.E.J., Desmond, J.E., Moore, J.W., and Berthier, N.E. Simulation of the classically conditioned response by a neuron-like adaptive element: A real-time variant of the Sutton-Barto model. *Proceedings of the eighth annual conference of the Cognitive Science Society*. Hillsdale, N.J.: Lawrence Erlbaum Associates, 1986, 176-186.

Bloedel, J.R. and Ebner, T.J. Climbing fiber function: regulation of Purkinje cell responsiveness. In J.R. Bloedel, J. Dichgans, and W. Precht (Eds.), *Cerebellar functions*. New York: Springer-Verlag, 1985, 247-260.

Bloedel, J.R. and Roberts, W.J. Functional relationships among neurons of the cerebellar cortex in the absence of anesthesia. *Journal of Neurophysiology*, 32: 75-82 (1969).

Brodal, P., Dietrichs, E., and Walberg, F. Do pontocerebellar mossy fibres give off collaterals to the cerebellar nuclei? An experimental study in the cat with implantation of crystalline HRP-WGA. *Neuroscience Research*, 4: 12-24 (1986).

Buchtel, H.A., Iosif, G., Marchesi, G.F., Provini, L., and Strata, P. Analysis of the activity evoked in the cerebellar cortex by stimulation of the visual pathways. *Experimental Brain Research*, 15: 278-288 (1972).

Churchland, P. *Neurophilosophy*. Cambridge, Mass: MIT Press, 1986.

Clark, G.A., McCormick, D.A., Lavond, D.G. and Thompson, R.F. Effects of lesions of cerebellar nuclei on conditioned behavioral and hippocampal neuronal responses. *Brain Research*, 291: 125-136 (1984).

Desmond, J.E. *The classically conditioned nictitating membrane response: analysis of learning-related single neurons of the brain stem*, Ph.D. dissertation, University of Massachusetts, 1985.

Desmond, J.E., Blazis, D.E.J., Moore, J.W., and Berthier, N.E. Computer simulations of a classically conditioned response using neuron-like adaptive elements: Response topography. *Society for Neuroscience Abstracts*, 12: 516 (1986).

Desmond, J.E. and Moore, J.W. A brain stem region essential for the classically conditioned but not unconditioned nictitating membrane response. *Physiology & Behavior*, 28: 1029-1033 (1982).

Desmond, J.E. and Moore, J.W. Dorsolateral pontine tegmentum and the classically conditioned nictitating membrane response: analysis of CR-related single-unit activity. *Experimental Brain Research*, 65: 59-74 (1986).

Desmond, J.E. and Moore, J.W. Simulating conditioned response topography: A network approach. Presented at the *Conference on Neural Models of Plasticity: Theoretical and Empirical Approaches*. Woods Hole, Massachusetts, April 29–May 1, 1987.

Donegan, N.H. and Wagner, A.R. Conditioned diminution and facilitation of the UR: A sometimes opponent-process interpretation. In I. Gormezano, W.F. Prokasy, and R.F. Thompson (Eds.), *Classical conditioning, 3rd edition.* Hillsdale, N.J.: Lawrence Erlbaum Associates, 1987, 339-369.

Durand, J., Gogan, P., Gueritaud, J.P., Horcholle-Bossavit, G., and Tyc-Dumont, S. Morphological and electrophysiological properties of trigeminal neurones projecting to the accessory abducens nucleus of the cat. *Experimental Brain Research*, 53: 118-126 (1983).

Eccles, J.C., Sasaki, K., and Strata, P. A comparison of the inhibitory action of Golgi and basket cells. *Experimental Brain Research*, 3: 81-94 (1967).

Gamble, E. and Koch, C. The dynamics of free calcium in dendritic spines in response to repetitive synaptic input. *Science*, 236: 1311-1315 (1987).

Gormezano, I., Kehoe, E.J., and Marshall, B.S. Twenty years of classical conditioning with the rabbit. In J.M. Sprague and A.N. Epstein (Eds.), *Progress in Psychobiology and Physiological Psychology*, 10: 197-275 (1983).

Grant, K. and Horcholle-Bossavit, G. Red nucleus inputs to retractor bulbi motoneurons in the cat. *Journal of Physiology (London)*, 371: 317-327 (1986).

Hassul, M. and Daniels, P.D. Cerebellar dynamics: The mossy fiber input. *IEEE Transactions on Biomedical Engineering*, BME-24: 449-456 (1977).

Hawkins, R.D. and Kandel, E.R. Is there a cell-biological alphabet for simple forms of learning? *Psychological Review*, 91: 375-391 (1984).

Hoehler, F.K. and Thompson, R.F. Effect of the interstimulus (CS-US) interval on hippocampal unit activity during classical conditioning of the nictitating membrane response of the rabbit. *Journal of Comparative and Physiological Psychology*, 94: 201-215 (1980).

Ikeda, M. Projections from the spinal and principal sensory nuclei of the trigeminal nerve to the cerebellar cortex in the cat, as studied by retrograde transport of horseradish peroxidase. *Journal of Comparative Neurology*, 184: 567-586 (1979).

Ito, M. *The cerebellum and neural control.* New York: Raven, 1984.

Kehoe, E.J. and Gormezano, I. Effects of trials per session on conditioning of the rabbit's nictitating membrane response. *Bulletin of the Psychonomic Society*, 2(4B): 434-436 (1974).

Kelso, S.R., Ganong, A.H., and Brown, T.R. Hebbian synapses in hippocampus. *Proceedings of the National Academy of Science (USA)*, 83: 5326-5330 (1986).

Lisberger, S.G., Morris, E.J., and Tychsen, L. Visual motion processing and sensory-motor integration for smooth pursuit eye movements. *Annual Review of Neuroscience.* 10: 97-129 (1987).

Liu, S.S. and Moore, J.W. Auditory differential conditioning of the rabbit nictitating membrane response: IV. Training based on stimulus offset and the effect of an intertrial tone. *Psychonomic Science*, 15: 128-129 (1969).

Llinas, R. Neuronal operations in cerebellar transactions. In F.O. Schmitt (Ed.), *The neurosciences: second study program*, New York: Rockefeller University Press, 1970, 409-426.

Llinas, R. Functional significance of the basic cerebellar circuit in motor coordination. In J.R. Bloedel, J. Dichgans, and W. Precht (Eds.), *Cerebellar functions.* New York: Springer-Verlag, 1985, 230-247.

Mackintosh, N.J. *Conditioning and associative learning.* New York: Oxford University Press, 1983.

Marr, D. A theory of cerebellar cortex. *Journal of Physiology (London)*, 202: 437-470 (1969).

Miles, F.A., Fuller, J.H., Braitman, D.J., and Dow, B.M. Long-term adaptive changes in primate vestibuloocular reflex. III. Electrophysiological observations in flocculus of normal monkeys. *Journal of Neurophysiology*, 43: 1437-1476 (1980).

Mis, F.W. A midbrain-brain stem circuit for conditioned inhibition of the nictitating membrane response in the rabbit (*Oryctolagus cuniculus*). *Journal of Comparative and Physiological Psychology*, 91: 975-988 (1977).

Moore, J.W. and Desmond, J.E. Latency of the nictitating membrane response to periocular electrostimulation in unanesthetized rabbits. *Physiology & Behavior*, 28: 1041-1046 (1982).

Moore, J.W., Desmond, J.E., Berthier, N.E., Blazis, D.E.J., Sutton, R.S., and Barto, A.G. Simulation of the classically-conditioned nictitating membrane response by a neuron-like adaptive element: response topography, neuronal firing, and interstimulus intervals. *Behavioural Brain Research*, 12: 143-154 (1986).

Moore, J.W. and Gormezano, I. Classical conditioning. In M.H. Marx and M.E. Bunch (Eds.), *Fundamentals and applications of learning*. New York: Macmillan, 1977, 87-120.

Moore, J.W. and Stickney, K.J. Antiassociations: Conditioned inhibition in attentional-associative networks. In Miller, R. R. and Spear, N.E. (Eds.), *Information processes in animals: conditioned inhibition*. Hillsdale, N. J.: Lawrence Erlbaum Associates, 1985, 209-222.

Palay, S.L. and Chan-Palay, V. *Cerebellar cortex: cytology and organization*. New York: Springer-Verlag, 1974.

Pavlov, I.P. *Conditioned reflexes*. London: Oxford University Press, 1927.

Port, R.L., Mikhail, A.A., and Patterson, M.M. Differential effects of hippocampectomy on classically conditioned rabbit nictitating membrane response related to interstimulus interval. *Behavioral Neuroscience*, 99: 200-208 (1985).

Port, R.L., Romano, A.G., Steinmetz, J.E., Mikhail, A.A., and Patterson, M.M. Retention and acquisition of classical trace conditioned responses by hippocampal lesioned rabbits. *Behavioral Neuroscience*, 100: 745-752 (1986).

Robinson, F.R., Houk, J.C., and Gibson, A.R. Limb specific connections of the cat magnocellular red nucleus. *Journal of Comparative Neurology*, 257: 553-577 (1987).

Rosenfield, M.E., Dovydaitis, A., and Moore, J.W. Brachium conjunctivum and rubrobulbar tract: Brain stem projections of red nucleus essential for the conditioned nictitating membrane response. *Physiology & Behaviour*, 34: 751-749 (1985).

Salafia, W.R., Lambert, R.W., Host, K.C., Chiaia, N.L., and Ramirez, J.J. Rabbit nictitating membrane conditioning: Lower limit of effective interstimulus interval. *Animal Learning & Behavior*, 8: 85-91 (1980).

Schmajuk, N.A. *Real-time attentional models for classical conditioning and the hippocampus*, Ph.D. dissertation, University of Massachusetts, 1986.

Schmajuk, N.A. and Moore, J.W. A real-time attentional-associative network for classical conditioning of the rabbit's NMR. *Proceedings of the eighth annual conference of the Cognitive Science Society* . Hillsdale, N.J.: Lawrence Erlbaum Associates, 1986, 794-807.

Schneiderman, N. Interstimulus interval function of the nictitating membrane response of the rabbit under delay versus trace conditioning. *Journal of Comparative and Physiological Psychology*, 62: 397-402 (1966).

Schulman, J.A. and Bloom, F.E. Golgi cells of the cerebellum are inhibited by inferior olive activity. *Brain Research*, 210: 350-355 (1981).

Shofer, R.J. and Nahvi, M.J. Firing patterns induced by sound in single units of cerebellar cortex. *Experimental Brain Research*, 8: 327-345 (1969).

Smith, M.C., Coleman, S.R., and Gormezano, I., Classical conditioning of the rabbit's nictitating membrane response at backward, simultaneous, and forward CS-US intervals. *Journal of Comparative and Physiological Psychology*, 69: 226-231 (1969).

Snider, R.S. and Stowell, A. Receiving areas of tactile, auditory, and visual systems in the cerebellum. *Journal of Neurophysiology*, 7: 331-357 (1944).

Solomon, P.R., Vander Schaaf, E.R., Norbe, A.C., Weisz, D.J., and Thompson, R.F. Hippocampus and trace conditioning of the rabbit's nictitating membrane response. *Behavioral Neuroscience*, 100: 729-744 (1986).

Spacek, J., Parizek, J., and Lieberman, A.R. Golgi cells, granule cells and synaptic glomeruli in the molecular layer of the rabbit cerebellar cortex. *Journal of Neurocytology* 2: 401-428 (1973).

Stent, G.S. A physiological mechanism for Hebb's postulate of learning. *Proceedings of the National Academy of Science (USA)*, 70: 997-1001 (1973).

Strata, P. Inferior olive: Functional aspects. In J.R. Bloedel, J. Dichgans, and W. Precht (Eds.), *Cerebellar functions*. New York: Springer-Verlag, 1985, 230-246.

Sutton, R.S. and Barto, A.G. Toward a modern theory of adaptive networks: Expectation and prediction. *Psychological Review*, 88: 135-170 (1981).

Sutton, R.S. and Barto, A.G. A temporal-difference model of classical conditioning. Technical Report TR87-509.2, GTE Labs, Waltham, Mass. (1987).

Tesauro, G. Simple neural models of classical conditioning. *Biological Cybernetics*, 55: 187-200 (1986).

Thach, W.T. Somatosensory fields of single units in cat cerebellar cortex. *Journal of Neurophysiology*, 30: 675-696 (1967).

Thompson, R.F. The neurobiology of learning and memory. *Science*, 233: 941-947 (1986).

Thompson, R.F., Donegan, N.H., Clark, G.A., Lavond, D.G., Lincoln, J.S., Madden, J., Mamounas, L.A., Mauk, M.D., and McCormick, D.A. Neuronal substrates of discrete, defensive conditioned reflexes, conditioned fear states, and their interactions in the rabbit. In I. Gormezano, W.F. Prokasy, and R.F. Thompson (Eds.), *Classical conditioning, 3rd edition*. Hillsdale, N.J.: Lawrence Erlbaum Associates, 1987, 371-400.

Walters, E.T. and Byrne, J.H. Associative conditioning in single neurons suggests a cellular mechanism for learning. *Science*, 219: 405-408 (1983).

Yeo, C.H., Hardiman, M.J., and Glickstein, M. Discrete lesions of the cerebellar cortex abolish the classically conditioned nictitating membrane response. *Behavioural Brain Research*. 13: 261-266 (1984).

Yeo, C.H., Hardiman, M.J., and Glickstein, M. Classical conditioning of the nictitating membrane response of the rabbit. I. Lesions of the cerebellar nuclei. *Experimental Brain Research*, 60: 87-98 (1985a).

Yeo, C.H., Hardiman, M.J., and Glickstein, M. Classical conditioning of the nictitating membrane response of the rabbit. II. Lesions of the cerebellar cortex. *Experimental Brain Research*, 60: 99-113 (1985b).

Yeo, C.H., Hardiman, M.J., and Glickstein, M. Classical conditioning of the nictitating membrane response of the rabbit. III. Connections of cerebellar lobule HVI. *Experimental Brain Research*, 60: 114-126 (1985c).

Yeo, C.H., Hardiman, M.J., and Glickstein, M. Classical conditioning of the nictitating membrane response of the rabbit. IV. Lesions of the inferior olive. *Experimental Brain Research*, 63: 81-92 (1986).

Yeo, C.H., Hardiman, M.J., Moore, J.W., and Steele-Russell, I. Retention of conditioned inhibition of the nictitating membrane response in decorticate rabbits. *Behavioural Brain Research*, 10: 383-392 (1983).

END

DATE

FILMD

3 — 88

DTIC